Title

A Platform of Synthetic Lethal Gene Interaction Networks Reveals that the GNAQ Uveal Melanoma Oncogene Controls the Hippo Pathway through FAK

Journal

Cancer Cell, 35(3)

ISSN

1535-6108

Authors

Feng, Xiaodong
Arang, Nadia
Rigiracciolo, Damiano Cosimo
et al.

Publication Date

2019-03-01

DOI

10.1016/j.ccell.2019.01.009

Peer reviewed

HHS Public Access

Author manuscript

Cancer Cell. Author manuscript; available in PMC 2020 March 18.

Published in final edited form as:

Cancer Cell. 2019 March 18; 35(3): 457–472.e5. doi:10.1016/j.ccell.2019.01.009.

A Platform of Synthetic Lethal Gene Interaction Networks Reveals that the *GNAQ* Uveal Melanoma Oncogene Controls the Hippo Pathway through FAK

Xiaodong Feng[1,2,#], **Nadia Arang**[1,3,#], **Damiano Cosimo Rigiracciolo**[1,7], **Joo Sang Lee**[4,8,*], **Huwate Yeerna**[1], **Zhiyong Wang**[1,3], **Simone Lubrano**[1], **Ayush Kishore**[1], **Jonathan A. Pachter**[6], **Marcello Maggiolini**[7], **Evi Kostenis**[5], **David D. Schlaepfer**[1], **Pablo Tamayo**[1,9], **Qianming Chen**[2,*], **Eytan Ruppin**[4,8,*], **J. Silvio Gutkind**[1,*]

[1]Moores Cancer Center, University of California, San Diego, La Jolla, CA 92093, USA

[2]State Key Laboratory of Oral Diseases, National Clinical Research Center for Oral Diseases, West China Hospital of Stomatology, Sichuan University, Chengdu, 610041, China

[3]Biomedical Sciences Graduate Program, University of California, San Diego, La Jolla, CA 92093, USA

[4]Cancer Data Science Lab, National Cancer Institute, National Institute of Health, MD, 20892, USA

[5]Molecular, Cellular and Pharmacobiology Section, Institute of Pharmaceutical Biology, University of Bonn, 53115 Bonn, Germany

[6]Verastem Oncology, Needham, MA, USA

[7]Department of Pharmacy and Health and Nutritional Sciences, University of Calabria, Rende 87036, Italy

[8]Center for Bioinformatics and Computational Biology & Department of Computer Sciences, University of Maryland, College Park, MD, 20742, USA

[9]Division of Medical Genetics, UC San Diego School of Medicine, La Jolla, CA 92093, USA

SUMMARY:

[*]Senior Authors: Correspondence: qmchen@scu.edu.cn (Q.C.), lee.joosang@gmail.com (JSL), eyruppin@gmail.com (E.R.), sgutkind@ucsd.edu (J.S.G.).

[#]Co-first authors

AUTHOR CONTRIBUTIONS

Conceptualization, X.F., E.R. and J.S.G.; Methodology, X.F., J.S.G., J.S.L., E.R., H.Y. and P.T; Investigation, X.F., D.C.R., J.S.L., H.Y., N.A., Z.W., S.L. and A.K.; Formal Analysis, X.F., N.A., D.C.R., J.S.L. and H.Y.; Resources, J.S.L., J.P., E.K., Q.C. M.M. and D.D.S. Writing – Original Draft, X.F., N.A. J.S.L. and J.S.G.; Writing – Review & Editing, X.F., N.A., E.K., D.D.S., P.T., E.R. and J.S.G; Visualization, X.F., D.C.R., J.S.L., H.Y. and J.S.G.; Funding Acquisition, M.M., D.D.S, P.T., Q.C., X.F., E.R. and J.S.G.; Supervision, J.S.G.

Lead Contact: J. Silvio Gutkind, Professor, Department of Pharmacology, Associate Director of Basic Science, UC San Diego Moores Cancer Center, 3855 Health Sciences Drive, #0803, La Jolla, CA 92093

DECLARATION OF INTERESTS

J.A.P is an employee (Chief Scientific Officer) of VERASTEM, INC., which has not influenced this study. Other authors declare no competing financial interests.

Activating mutations in *GNAQ/GNA11,* encoding Gαq G-proteins, are the cancer initiating oncogenes in uveal melanoma (UM). However, there are no effective therapies for UM. Using an integrated bioinformatics pipeline, we found that *PTK2,* encoding Focal Adhesion Kinase (FAK), represents a candidate synthetic lethal gene with *GNAQ* activation. We show that Gαq activates FAK through TRIO-RhoA non-canonical Gαq-signaling, and genetic ablation or pharmacological inhibition of FAK inhibits UM growth. Analysis of the FAK-regulated transcriptome demonstrated that *GNAQ* stimulates YAP through FAK. Dissection of the underlying mechanism revealed that FAK regulates YAP by tyrosine phosphorylation of MOB1, inhibiting core Hippo signaling. Our findings establish FAK as a novel precision therapeutic target for UM and other Gαq-driven pathophysiologies that involve unrestrained YAP function.

IN BRIEF:

An integrated bioinformatics analysis of predicted synthetic lethality and gene interaction networks reveals FAK as a key mediator of the cancer-promoting signaling circuitry initiated by GNAQ, the uveal melanoma oncogene. Gaq, encoded by GNAQ, activates FAK by a non-canonical signaling pathway, and in turn FAK activates YAP by a novel mechanism suppressing the Hippo kinase cascade. Further in vivo analysis establishes FAK as a viable precision therapeutic target for the treatment of uveal melanoma, a cancer that lacks effective targeted therapies.

GRAPHICAL ABSTRACT

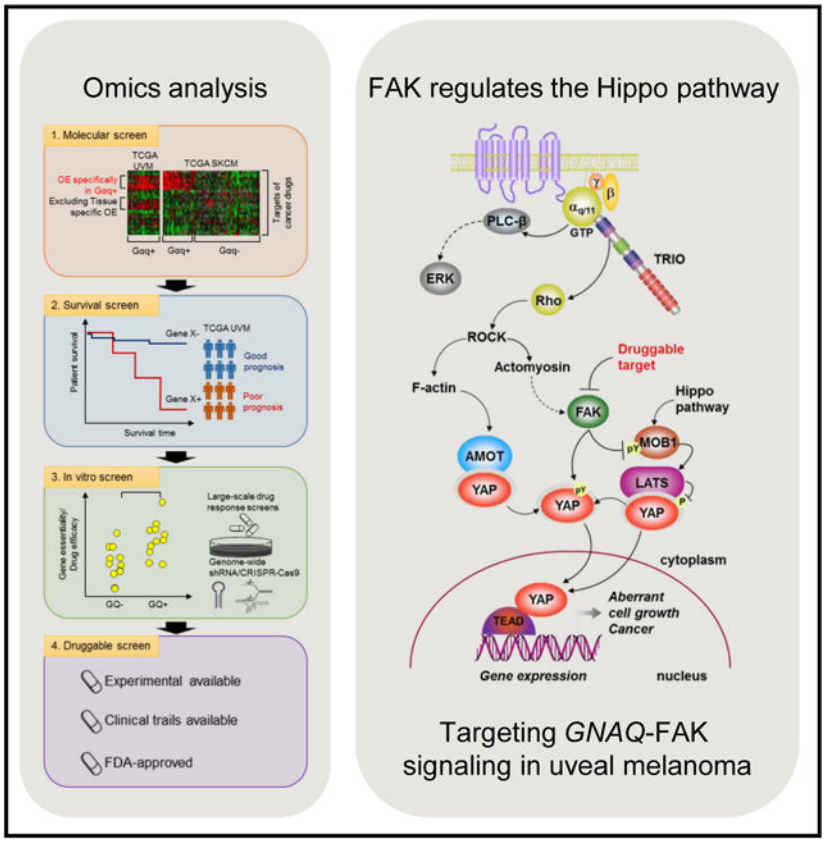

Keywords

GNAQ/GNA11; *PTK2*; FAK; YAP; Hippo; MOB1; G protein; signal transduction; Uveal Melanoma

INTRODUCTION:

Recent advances in omics technologies have enabled the sequencing and characterization of cancers to an unprecedented depth, revealing novel mechanisms of growth and molecular drivers of disease. Bioinformatics analyses of these data have demonstrated a large heterogeneity in genetic drivers, highlighting complex biological networks towards the identification of therapeutic targets. These large-scale genomics efforts have revealed a small set of cancers that are driven by only a select number of mutational events. One such cancer, uveal melanoma (UM), is characterized by a gain of function mutation in the heterotrimeric G protein, Gαq. A hotspot mutation in *GNAQ* or *GNA11* encodes constitutively active Gαq proteins rendering them as driver oncogenes in approximately 93% of UM (Van Raamsdonk et al., 2009; Van Raamsdonk et al., 2010). Another ~4% of UM harbor activating mutations in *CYSLTR2,* a Gαq-linked G protein coupled receptor (GPCR) (Moore et al., 2016) firmly establishing UM as a Gαq-driven malignancy.

Aberrant activity of G proteins and GPCRs have been frequently associated with an oncogenic state and promotion of tumorigenesis (Dorsam and Gutkind, 2007; O'Hayre et al., 2013). However, the precise molecular mechanisms by which prolonged Gaq signaling controls cancer cell growth are under current investigation. We and others have previously shown that these mechanisms are in part due to unique signaling circuitries that lead to the activation of YAP, a transcriptional co-activator regulated by the Hippo pathway. In turn, YAP activation is necessary for UM growth (Feng et al., 2014b; Yu et al., 2014a). As a key downstream target of the tumor suppressive Hippo signaling cascade, YAP is typically over-activated in multiple cancers (Moroishi et al., 2015; Yu et al., 2015). Despite this, pharmacological targeting of YAP or the Hippo pathway has been proven to be challenging. Verteporfin, an ophthalmological drug, inhibits YAP-TEAD interaction, which is the major transcriptional factor regulated by YAP, in UM (Feng et al., 2014b; Yu et al., 2014a) with some anecdotal clinical success (Barbazetto et al., 2003; Soucek and Cihelkova, 2006); however, its potential as a therapeutic candidate has been hindered due to high systemic toxicities after prolonged use (Arnold et al., 2004; Azab et al., 2004). Currently, no effective therapeutic targets are available for UM, and no specific YAP inhibitors are currently in clinical use (Moroishi et al., 2015). As such, full dissection of Hippo/YAP- regulating mechanisms in cancer could identify urgently needed therapeutic opportunities to inhibit YAP-dependent tumor growth in UM and other cancer types.

The highly distinctive and well defined genetic landscape of UM provides a unique opportunity for the application of unbiased bioinformatics approaches to investigate the precise molecular mechanisms by which prolonged Gαq signaling controls cancer cell growth, and how these pathways can be targeted for precision therapies of Gαq-driven pathophysiologies. Here, we applied a novel computational framework to predict synthetic

lethal gene interactions of Gαq activation (that is, *synthetic dosage lethalities* of Gαq). Taking advantage of publicly available large-scale genomics and patient data sets included in The Cancer Genome Atlas (TCGA) (Cancer Genome Atlas Research et al., 2013), and related efforts, our pipeline searches for the drug targets that lead to selective death or growth suppression specifically in Gαq-activated tumors. These studies revealed that the *PTK2* gene, encoding the non-receptor tyrosine kinase known as focal adhesion kinase (FAK), is strictly required for UM cell growth and survival, and the dissection of the underlying mechanism led to the finding that FAK acts as a key mediator of Gαq-driven signaling to YAP. Moreover, we discovered that FAK regulates YAP activation through inhibition of Hippo signaling by the direct tyrosine phosphorylation of MOB1, a component of the core Hippo kinase pathway, and YAP. Finally, we demonstrate that targeting the Gαq-FAK- Hippo/YAP signaling axis by inhibition of FAK blocks YAP-dependent growth in UM, thereby establishing FAK as a novel viable therapeutic target for the treatment of this aggressive human malignancy.

RESULTS:

A novel bioinformatics pipeline identifies *PTK2* (encoding FAK), as a druggable candidate synthetic lethal gene with *GNAQ*.

To identify the specific vulnerabilities of GNAQ-driven tumor, we adapted our recently established bioinformatics pipeline that Identifies clinically relevant Synthetic Lethal Interactions (termed ISLE, (Lee et al., 2018)). We denote a sample with mutations or gene amplification of *GNAQ, GNA11* and *CYSLTR2* as Gαq+, while a sample with the absence of these GNAQ, *GNA11* or *CYSLTR2* gene alterations as Gαq-. Adapting the rationale of the ISLE pipeline to our specific aim here, a candidate gene was determined to be a synthetic lethal (and thus a druggable vulnerability) of Gαq+ tumors if it satisfies the following four conditions (Fig. 1A): (i) *molecular condition:* Gαq+ tumor should differentially overexpress the candidate gene *vs* Gαq-samples (ii) *clinical condition:* Overexpression of the candidate gene should be associated poor survival in Gαq+ tumors, (iii) *phenotypic condition:* The candidate gene is significantly more essential in Gαq+ than in Gαq-cell lines, (iv) *druggable condition:* Targeting the candidate gene with inhibitors is significantly more effective in Gαq+ than in Gαq-cell lines.

In more details, our analysis has proceeded along these four steps as follows: (i) First, taking advantage of the publicly available cancer genome atlas (TCGA) data, we extracted those genes that are differentially overexpressed in Gαq+ UM samples (>96%). Since there are no sufficient UM Gαq-samples, we used Gαq- samples of skin cutaneous melanoma (SKCM) as a control. Indeed, we observed significant overlap in the overexpressed genes in UM Gαq + and SKCM Gαq+ samples (hypergeometric $p<4.83\ e^{-199}$, see Methods) compared to SKCM Gαq-samples, justifying the use of SKCM Gαq-samples as a control for Gαq+ UM. We excluded the genes overexpressed in UM compared to SKCM samples irrespective of Gαq status to control for cancer type-specific differential expression (see Methods). (ii) Second, among the genes that pass the first filter, we identified the genes whose expression correlates with poor prognosis of UM patients (see Methods). (iii) Third, we further selected those genes from *in vitro* functional screens that show significantly higher essentiality (or

drug response) in the context of Gαq+ cancer cell lines following the standard procedure to determine cancer cell dependency (Tsherniak et al., 2017). (iv). Lastly, we selected only those genes that are druggable, i.e. targets of known cancer drugs (Fig. 1A, n=7). We performed cell viability assays after siRNA mediated gene expression inhibition, confirming the vulnerabilities of our predicted hits in Gαq+ cells (Fig. 1B). This four steps Gαq+ SL identification process results in 7 predicted SL genes, which play roles in multiple biological processes, including, cell growth, cell survival, lipid metabolism regulation, cell cycle control and the processing of class I MHC peptide, all of which showed reduced cell growth when knocked down. Among them, the top predicted gene, *PTK2*, also known as Focal Adhesion Kinase (FAK) reduced cell viability almost 60% after inhibition using *PTK2* specific siRNA knockdown (Fig. 1B).

PTK2 itself is not mutated in UM, a disease that is characterized by mutations, primarily mutually-exclusive activating mutations in *GNAQ, GNA11* and *CYSLTR2,* and mutually exclusive mutations in genes encoding two RNA splicing factors, *EIF1AX* and *SF3B1,* or a deubiquitinase *BAP1* (Moore et al., 2016; Robertson et al., 2017; Van Raamsdonk et al., 2009; Van Raamsdonk et al., 2010). Instead, statistically significant gain of chromosome 8q (Robertson et al., 2017), including *PTK2* and *MYC,* occurs in UM. Interestingly, *PTK2* and *MYC* are amplified in 18% of UM patients (TCGA), and 38% of UM patients also exhibit *PTK2* mRNA upregulation independent of amplification (Fig. 1C). In total 56% of UM patients have alterations in *PTK2* resulting in gene amplification or mRNA upregulation (Fig. 1C). Interestingly, we found that expression of FAK is significantly correlated with reduced overall patient survival (Fig. 1D). Strikingly, a pan-cancer analysis of alteration frequency of FAK reveals that UM has the highest alteration frequency among all available TCGA solid tumor cohorts (Fig. S1A). We next tested the sensitivity of five representative UM cell lines, 92.1, OMM1.3, OMM1.5, Mel270, and Mel202, all of which harbor *GNAQ* mutations, to FAK inhibition using VS-4718, a new generation orally-bioavailable FAK inhibitor (FAKi) (Sulzmaier et al., 2014), using an SKCM cell line SK-MEK-28 *(BRAF* mutant) as a control (Fig. 1E). *In vitro,* UM cell lines demonstrate a dose-dependent sensitivity to FAK inhibition with an EC_{50} of around 1μM (Fig. 1E). Similar results were obtained with PF562771, a chemically distinct FAKi (Fig. S1B). Instead, the SKCM cell line SK-MEK-28 *(BRAF)* was largely insensitive to FAKi, with an EC_{50}>10μM for VS-4718 (Fig. 1E). siRNA knockdown of *PTK2* reduced cell viability in two representative UM cells nearly as potently as *GNAQ* knock down (Fig. S1C, D, E and F). *GNAQ* knock down reduced the accumulation of FAK in its active, tyrosine 397 phosphorylated form (pY397-FAK) (Sulzmaier et al., 2014) (Fig. S1D), while FAK knock down reduced total FAK and pY397-FAK protein levels, as expected (Fig. S1E). FAKi inhibited FAK rapidly (Fig. 1F and S1G), and resulted in UM apoptosis as judged by the accumulation of cleaved PARP (Fig. 1F). We further assessed whether inhibition of FAK impacted the oncogenic potential of UM cells by measuring their clonogenic capacity in semisolid media, an assay often used to assess cancer stem cell properties. We found that FAKi nearly abolished the colony formation ability of UM cells (Fig. 1G). Together, these findings support that FAK may be required for *GNAQ*-driven UM cell proliferation, survival, and clonogenic growth, thereby representing a potential therapeutic target for the treatment of UM.

The canonical PLCβ/PKC Gαq signaling pathway is dispensable for FAK activation: Evidence for a TRIO-RhoA non-canonical signaling mechanism.

We next sought to investigate the mechanism by which Gαq controls FAK. To understand the impact of *GNAQ* mutation on FAK activation, we transfected human embryonic kidney 293 (HEK293) cells with an HA-tagged activated mutant of *GNAQ* observed in UM, encoding Gαq-Q209L (HA-GαqQL), and an empty vector control. Immunoblotting against total and phosphorylated forms of FAK revealed that phosphorylation of FAK at Y397 was significantly increased after transfection with GαqQL (Fig. 2A). We next took advantage of a previously established synthetic Gαq-coupled GPCR (Gαq-DREADD) that can be solely activated by a synthetic ligand, Clozapine N-oxide (CNO) (Armbruster et al., 2007; Vaque et al., 2013). We stimulated Gαq-DREADD expressing HEK293 cells with CNO over a time course and found increasingly elevated levels of pY397 FAK in response to CNO (Fig. 2B). In UM cells, *GNAQ* siRNA knockdown or inhibition by FR900359 (FR), a potent Gαq inhibitor (Schrage et al., 2015), diminished FAK and ERK activation (Fig. 2C and see above, Fig. S1D). Consistent with these data, Gαq inhibition with FR in UM cells and SKCM cells showed inhibition of cell proliferation exclusively in UM cells (Fig. 2D). These results support the emerging notion that FAK acts downstream from the *GNAQ* oncogene in UM. However, it is unclear which of the multiple Gαq or Gαq coupled receptor-initiated signaling pathways are responsible for regulating FAK activation.

PLCβ-dependent second messenger activation is among the best-known downstream events stimulated by Gαq (Griner and Kazanietz, 2007; Hubbard and Hepler, 2006), and is considered to be the canonical Gαq signaling pathway, causing transient ERK activation (Vaque et al., 2013). Inhibition of PLCβ by the use of a small-molecule PLC inhibitor (PLCi) abolished the ERK activation, as we previously reported (Vaque et al., 2013), but did not have an impact on the activation of FAK (Fig. 2E). Similarly, inhibition of PKC blocked ERK activation but not FAK in UM cells (Fig. 2F), indicating that FAK may be activated independently of PLCβ. As Gαq activation of the AP1 and YAP transcriptional programs involves the stimulation of the TRIO guanine nucleotide exchange factor (GEF) for Rho GTPases (Feng et al., 2014b; Vaque et al., 2013), we next asked if this non-canonical Gαq signaling pathway is involved in FAK activation by Gαq. Knockdown of *TRIO* or *RHOA* prevented the activation of FAK by Gαq-DREADD in HEK293 cells and *GNAQ* in UM cells (Fig. 2G and H). In line with these findings, knockdown of *RAC1* had no impact on FAK activation (Fig. 2G). Further analysis showed that blocking actin polymerization by inhibiting ROCK or actomyosin contraction by Y-27632 (Ikeda et al., 2003; Narumiya et al., 2000) and blebbistatin (Kovacs et al., 2004), respectively, repressed FAK activation by Gαq-DREADD in HEK293 cells and *GNAQ* in UM cells (Fig. 2I and J). Together, these findings suggest that Gαq stimulates FAK independently of PLCβ and PKC, but instead Gαq activates FAK through a non-canonical TRIO-dependent pathway resulting in RHOA activation and consequent cytoskeletal changes and actomyosin-initiated cell contraction and signaling (Fig. 2K).

FAK inhibition represses the transcriptional activity of YAP.

FAK is at the intersection of multiple signaling pathways that promote cancer progression (Sulzmaier et al., 2014), but it is not clear which downstream targets of FAK play a critical

role in UM. As an approach to identify key downstream targets of the Gαq-FAK signaling axis, we performed transcriptomic RNA-sequencing on UM cells treated with FAKi, and performed Gene Set Enrichment Analysis (GSEA)(Subramanian et al., 2005) to characterize the transcriptional effects of inhibiting Gαq and FAK at the pathway level using over 10,000 gene sets from the MSigDB *(Molecular Signatures Database),* including two sub-collections of oncogenic signatures and hallmark gene sets that our team has added to the database recently (Liberzon et al., 2015). In spite of this large collection of transcriptional regulated genes, only 20 oncogenic signature gene sets were significantly repressed and 5 were activated by FAKi in UM cells (Fig. 3A and S2A). These include the downregulation of genes described as stimulated by *KRAS* and *EGFR,* and cytokines such as IL21 and IL15, consistent with the likely role in the activation of growth promoting pathways by FAK (Sulzmaier et al., 2014). FAKi also reduced the expression of genes repressed (KD) by JAK2, p53, and BMI, suggesting that FAK inhibition may trigger a p53-response and stimulate BMI and JAK2, all of which may contribute to FAK-dependent cell growth and warrant further investigation. One of the most remarkable observations was that FAKi treatment resulted in a significant downregulation of YAP-signature genes (Zhao et al., 2008) (Fig. 3A–D and S2A and B). The involvement of Hippo/YAP signaling in cancer progression, as well as previous work demonstrating the key role of YAP signaling in uveal melanoma (Feng et al., 2014b; Yu et al., 2014a; Yu et al., 2014b) led us to pursue this specific gene signature. To validate these findings, we performed qPCR for the classical YAP-target genes *CTGF* and *CYR61* in UM cells and found significant reduction in the presence of FAKi and knockdown of FAK or *GNAQ* (Fig. 3E and S2C and D). We also found that FAKi clearly diminished YAP nuclear accumulation through quantification of anti-YAP staining, and western blot analysis of nuclear and cytoplasmic cellular fractions (Fig. 3F and G and S2E). We further confirmed the functional impact of FAKi and FAK knock down on YAP by performing YAP/TAZ luciferase reporter assays, and using *GNAQ* inhibition and knock down as a control (Fig. 3H–K, see Fig. S1D and E for knock down validation). Interestingly, inhibition of Gαq or FAK or siRNA-mediated FAK knockdown repressed YAP phosphorylation on tyrosine 357 (Y357), a residue that is associated with YAP activation (Li et al., 2016; Taniguchi et al., 2015), and increased phosphorylation on serine 127 (S127), which is one of the main repressive targets of Hippo signaling (Pan, 2010) (Fig. 3I and K). We recapitulated these findings in heterologous systems, using HEK293 cells expressing Gαq-DREADD stimulated with CNO and HEK293 cells transfected with GαqQL. In both cases, FAK inhibition or knockdown reduced YAP pY357 and increased pS127, and reduced mRNA levels of YAP targets and YAP activity measured by luciferase reporter assay (Fig. S2F–J), similar to UM cells. Inhibition of SRC in UM cells had no impact on YAP activity, measured by YAP/TAZ luciferase reporter assay, and failed to promote changes in YAP phosphorylation status (Fig. 3J and K). Together, these results suggest that Gαq and FAK regulate YAP activation in UM, and that this process is likely independent of SRC.

FAK regulates YAP activation through YAP tyrosine phosphorylation and inhibition of Hippo core kinases: A novel role for MOB1 tyrosine phosphorylation.

We sought to further investigate the impact of FAK on YAP activity via YAP/TAZ luciferase reporter assay and found that overexpression of FAK in HEK293 cells leads to a significant

increase of YAP activity (Fig. 4A). It is well-established that YAP activity and stability is tightly controlled by its phosphorylation status on a number of key phosphorylation sites (Moroishi et al., 2015; Yu et al., 2015). To define the phosphorylation state of YAP in the context of aberrant Gαq signaling, we transfected HEK293 cells with GαqQL as well as active FAK *in vitro.* Overexpression of GαqQL or FAK led to an increase in total levels of YAP protein, resulted in diminished YAP pS127, increased YAP pY357, and FAK alone was sufficient to stimulate YAP/TAZ luciferase reporter activity (Fig. 4 A, B and C). The latter results are aligned with our previous observations after FAKi (Fig. 3K), suggesting that FAK can promote tyrosine phosphorylation of YAP directly (see below, Fig. S4E).

Regarding the remarkable changes in YAP pS127 levels, we hypothesized that FAK may also repress inhibitory signals to YAP from the Hippo pathway through direct phosphorylation on the core kinases of the Hippo pathway. In the canonical Hippo pathway, MST1/2 kinases bound to their regulatory protein SAV1 activate the LATS1/2 kinases (collectively referred to as LATS) as part of a complex with MOB1A/B. LATS in turn phosphorylates YAP (or in certain cells TAZ) at multiple serine residues, including pS127, leading to YAP inactivation by cytoplasmic retention and subsequent degradation (Moroishi et al., 2015; Pan, 2010; Yu et al., 2015). By a systematic analysis of the tyrosine phosphorylation status of each Hippo core kinase cascade component after co-transfection with FAK, we found only MOB1A to be tyrosine phosphorylated, as judged by its detection with anti-phosphotyrosine antibodies in tagged MOB1A immune precipitates (Fig. 4D). MOB1 plays a critical regulatory role in the Hippo signaling cascade by transferring the upstream signal from the kinase complex of MST1/SAV1 to LATS (Meng et al., 2016). Consistent with our findings, scanning through large phosphoprotein databases (PhosphoSitePlus® PTM Resource, Cell signaling technology), we found that Y26 on MOB1A/B is conserved among mammals, and that this particular residue is phosphorylated in numerous high-throughput phosphoproteomic datasets (n=161) (Fig. S3A). To interrogate the functional impact of this phosphorylation site (Y26) on MOB1, we transfected HEK293 cells with HA-MOB1 and performed anti-HA and anti-pY IPs. Firstly, we found that an antibody raised anti-pY26 MOB1 recognized MOB1 only when co-transfected with FAK, which was abolished upon mutation of Y26 residue on MOB1 to Y26F (Fig. 4E and4F), thus serving as a specificity control. We further verified that FAK was able to directly phosphorylate MOB1 on its Y26 site by *in vitro* kinase reaction using purified recombinant proteins (Fig. S3B). When exploring the consequences of this post translational modification in the assembly of Hippo kinase complexes, we found that phosphorylation on Y26-MOB1 by FAK dissociates the MOB1/LATS complex (Fig. 4E). Strikingly, mutation of Y26 residue on MOB1 to Y26F rescued the dissociation with LATS1 (Fig. 4F) and abolished YAP activation by FAK (Fig. S3C). Together, these data suggest that FAK regulates MOB1 Y26 phosphorylation, resulting in the dissociation of the functional MOB1/LATS complex, preventing Hippo-dependent inhibition of YAP and thereby promoting YAP activity.

FAK inhibition results in increased MOB1/LATS association and signaling, and reduced YAP protein stability in UM.

To study the effect of FAK inhibition on the Hippo pathway in UM cells, we examined the phosphorylation status of key Hippo pathway components after a time course of FAKi. We

observed an increase of pS127-YAP, p909-LATS1, p1079-LATS1, a dose-dependent decrease in pY26 MOB1, and in line with our previous data, enhanced MOB1/LATS interaction (Fig. 5A and B, and S4A). In contrast, the MOB1-Y26F mutant demonstrated constitutively strong interaction with LATS independent of FAKi treatment (Fig. S4B and C) and remarkably, expression of MOB1-Y26F in UM cells phenocopied FAKi treatment as it drastically diminished cell proliferation that could not be further reduced by FAKi (Fig. S4D). Of interest, however, we did not observe an increase in p-MST1 in response to FAK inhibition (Fig. 5A), nor a change in phosphorylation of MOB1 at T35, the main target of MST1 on MOB1 (Meng et al., 2016) with FAKi or knockdown of FAK (Fig. S4B and C). This suggests that in UM, FAK regulates the link between LATS1 and YAP through MOB1, acting downstream from MST1 rather than controlling MST1 (Hippo) activity. In conjunction, we found FAK was able to phosphorylate YAP at Y357 *in vitro*, (Fig. S4E), a post translational modification that has been shown to regulate YAP stability and activity (Li et al., 2016; Taniguchi et al., 2015), and aligned with this finding, that FAK inhibition also caused diminished phosphorylation of Y357-YAP in UM cells (Fig. 5A). Indeed, we confirmed that long-term (up to 36 hours) FAK inhibition caused YAP protein downregulation (Fig. 5C). Furthermore, LATS1/2 knockdown was sufficient to rescue from the growth inhibition by FAKi in UM cells (Fig. 5D), supporting that YAP signaling plays a key role in growth promotion downstream from FAK in UM cells. Altogether, our data suggest that FAK drives UM cell growth through promotion of YAP activity by coordinating the previously described the F-actin-mediated release of YAP from AMOT, which enhances the pool of cytosolic YAP and enables its nuclear translocation (Feng et al., 2014b), with the release of the inhibitory Hippo kinase cascade through the FAK-mediated phosphorylation of MOB1, and the concomitant tyrosine phosphorylation and stabilization of YAP (Fig. 5E).

FAK represents a therapeutic target in UM.

We next tested the preclinical potential of FAK inhibition for UM treatment. For these studies, we first used lentiviral-delivered Cas9-sg*PTK2* to knockout (KO) FAK expression in UM cells (Fig. 6A). Most UM cells did not survive after genome editing of FAK (not shown), only mass cultures of MEL270 targeted for FAK grew in culture after puromycin selection, displaying nearly abolished FAK protein levels (Fig. 6A). Re-expression of FAK under control of a doxycycline-inducible promoter was sufficient to rescue cell viability in UM cells in which FAK expression was reduced (Fig. S5A). We observed that FAK KO cells developed only very small tumors, clearly smaller than control cells (Fig. 6B), suggesting that FAK activation may represent a molecular event involved in UM tumor growth *in vivo.* These observations further support the therapeutic potential of targeting FAK for UM. While there are multiple FAKi under clinical evaluation (Sulzmaier et al., 2014), VS-4718, chosen for our studies, was specifically designed for oral administration. We found that FAKi reduces both UM tumor size and cell proliferation in two different UM tumor models, the latter clearly visible by Ki67 staining that was nearly absent in VS-4718 treated mice (Fig. 6C–F). We observed clearly increased cytoplasmic retention of YAP in FAKi treated tumors, consistent with our previous findings that FAK controls YAP-activity in UM cells (Fig. 6G and H). These results suggest that the pharmacological inhibition of FAK by VS-4718 may represent a viable therapeutic approach for the treatment of patients with UM harboring increased YAP activity.

DISCUSSION

The generation of massive quantities of genomic, epigenomic and proteomic data has greatly enhanced our understanding of oncogenesis and cancer as a cellular state. In particular, development of bioinformatics pipelines to predict previously unanticipated nodes of connectivity between transcriptional and signaling networks can significantly expedite efforts to identify and exploit molecular vulnerabilities for the treatment of cancer. We focused here on applying such methods to UM, as the constitutive activation of the Gαq pathway *via* a limited number of mutations is sufficient as a key oncogenic driver of this malignancy, such that targeting these network alterations may help reveal effective treatment options (in contrast to, e.g., SKCM, a related cancer but with high mutational burden (Robertson et al., 2017). We thus hypothesized that focusing on a cancer type specifically driven by few activating (Gαq) mutations may serve as a good testbed for studying such an approach, harnessing a novel SL-based integrated bioinformatics analysis to uncover novel oncogenic signaling mechanisms controlled by Gαq and target them. In this study, we demonstrate that FAK acts as a critical oncogenic signaling node in UM—mediating Gαq-driven regulation of the Hippo/YAP pathway and enabling the promotion of an oncogenic state. We provide evidence that FAK destabilizes interactions between key core Hippo pathway members thereby activating YAP in an MST1 (Hippo)-independent manner. Furthermore, we show that the oncogenic activity of FAK in UM is targetable by clinically relevant therapeutic agents.

The transformative potential of Gαq signaling was established in the early 1990s (Gutkind et al., 1991; Kalinec et al., 1992) however, the precise signaling events by which Gαq and its linked receptors transduce sustained proliferative signals is not yet well defined. This is due in part to the large number of second messenger generating systems and signaling events that can be perturbed upon Gαq activation. The activation of these second messenger systems and their direct targets, including ion channels and regulated kinases, such as PKC, CAMKs and MAPK are responsible for most of the rapid physiological responses elicited by GPCRs (Griner and Kazanietz, 2007; Howe, 2011; Julius and Nathans, 2012; Newton, 2010; Prevarskaya et al., 2011; Rozengurt, 2007; Sassone-Corsi). Recent studies have identified additional members of this network for UM, highlighting the role of GEFs such as RasGRP3 in MAPK activation (Chen et al., 2017). Despite this link, therapeutic strategies targeting MAPKs have proven to be unsuccessful. The MEK inhibitor selumetinib has been extensively evaluated for UM treatment; however, recent clinical trials demonstrated that MEK inhibition with this agent or trametinib, as single agents or in combination with Dacarbazine has nearly no impact on the overall survival of UM patients (Carvajal et al., 2018; Carvajal et al., 2014). This suggests that although MEK/MAPK networks activated by PLCβ may contribute to UM initiation, they may not be critical for the maintenance of tumorigenic potential in UM.

Contrary to the transient nature of signal transmission through PLCβ, unbiased genome-wide RNAi screens revealed that the signaling events driven by Gαq which result in aberrant cell proliferation that are dependent on highly specific protein-protein interactions, rather than solely on diffusible second-messenger systems. Specifically, prior systems biology approaches have identified the RhoGEF TRIO as critical for activating Gαq-driven AP-1-

regulated transcriptional networks independently of PLCβ to achieve sustained stimulation of proliferative pathways (Vaque et al., 2013). Further work has shown that this novel pathway converges in the activation of YAP, and that in turn, YAP activation is critical for oncogenic potential of UM (Feng et al., 2014a; Feng et al., 2014b; Yu et al., 2014a). The Hippo/YAP cascade is a key growth-regulating pathway in normal cellular physiology (Bhatt et al., 2010; Moroishi et al., 2015; Yu et al., 2015). Unsurprisingly, dysregulation of the Hippo pathway is seen frequently in cancer; however, core components are rarely mutated (Martin et al., 2018; Moroishi et al., 2015). Rather, external pressures from upstream oncogenes typically drive YAP-dependent cell proliferation. Identifying the key molecular players that facilitate oncogenic signaling through Hippo/YAP pathway may also uncover potential network vulnerabilities. Interestingly, inhibition of PLCβ does not impact the activation of YAP after Gαq stimulation (Feng et al., 2014b). Together, these findings suggest that the canonical Gαq-PLCβ-MAPK signaling axis may be critical for tumor initiation rather than tumor maintenance, and that opportunities for intervention may lie within the distinct signaling circuitry transduced through TRIO.

We sought to define the distinct molecular framework involved in UM tumor maintenance by taking advantage of a bioinformatics pipeline designed to identify molecular vulnerabilities based on the prediction of synthetic lethal genetic interactions. The top candidate of our screen, FAK, is a nonreceptor tyrosine kinase whose role as a downstream target of Gαq has been well established by biochemical studies (Gutkind and Robbins, 1992); however, the contribution of FAK as a mediator of oncogenic Gαq signaling has not been previously explored. Our finding that FAK is rapidly activated by Gαq-linked GPCRs and the *GNAQ* oncogene through TRIO and RHOA, rather than PLCβ, in experimental cellular systems and UM cells, prompted us to focus on the possibility that FAK may represent an integral component of the non-canonical pathway by which Gαq regulates aberrant cell growth. We found that FAK knock down and pharmacological inhibition is sufficient to reduce UM cell proliferation, and if prolonged, to trigger apoptotic cell death. This remarkable response was unanticipated, as FAK inhibitors often have limited activity as single agents in most cancers, but instead synergize with cytotoxic agents, as we have shown for ovarian cancer that overexpresses FAK, as a typical example (Sulzmaier et al., 2014). We hypothesized that as compared to other cancer types with FAK gene upregulation, the compounding impact of FAK copy number gain and gene upregulation and Gαq-driven FAK activity in UM, creates a unique cellular state which may be highly dependent on the activity of FAK and therefore highly sensitive to FAK inhibition. This unexpected convergence of computational predictions, biochemical, and genetic information enabled the discovery of the therapeutic potential of FAK inhibitors for UM treatment.

Our RNAseq studies examining the functional role of FAK in UM, revealed an enrichment of several oncogenic signatures including KRAS and EGFR-regulated genes; however, strikingly, YAP conserved signature was among the top hits. FAK has been recently linked to YAP activity in the context of mechanotransduction, as well as in the coordination of cell proliferation and differentiation in mouse incisors during development; however, the underlying cell-context specific and developmental mechanisms are still not fully understood (Hu et al., 2017; Lachowski et al., 2018). We provide evidence that in UM the role of FAK converges on promoting YAP activity through the tandem inhibition of Hippo pathway

signals by Y26 phosphorylation of MOB1, and the regulation of YAP by Y357 phosphorylation. In the case of YAP phosphorylation, these observations extend prior studies indicating the role of JAK2 and SRC tyrosine kinases in Y357 phosphorylation (Li et al., 2016; Taniguchi et al., 2015). However, downstream from FAK, we observed both tyrosine-phosphorylated YAP and a decrease in pS127 YAP, the latter a direct target of the Hippo signaling pathway. In this regard, there is increasing evidence suggesting that Hippo signaling is tightly regulated by the assembly and dissociation of key signaling complexes. Our interrogation of these complexes in response to FAK activation led to the finding that FAK phosphorylates MOB1 on Y26, resulting in the disassembly of the MOB1/LATS complex and disruption of the Hippo pathway downstream from MST1, effectively rewiring the cellular forces in control of YAP activity, and that mutation of this tyrosine residue is sufficient to abolish the effect of FAK. Whereas further work may be required to establish the structural basis for this inhibition, as well as alternative FAK-driven pathways in mechanotransduction and development, our findings support that disruption of the MOB1/LATS signaling complex by FAK is a key regulatory step resulting in YAP activation by Gαq. Ultimately, this novel mechanism may coordinate the Gαq-induced increase in cytosolic free YAP, which is mediated by Rho-induced actin polymerization (Feng et al., 2014b), with Hippo kinase cascade inhibition through the FAK-mediated phosphorylation of MOB1, resulting in the YAP-dependent UM cell growth.

The current lack of effective approved targeted treatments for primary or metastatic UM leaves a large therapeutic gap for patients and clinicians underscoring an urgent need for the identification of novel pharmacological targets for therapeutic intervention in diseases involving persistent Gαq signaling. As YAP-targeting strategies have remained elusive thus far, the success of FAK inhibition in our *in vivo* models in the context of previously established success and safety of FAK inhibitors in human clinical trials highlight the direct translational potential of our findings and establish FAK as a novel precision therapeutic target for the treatment of UM. Towards this end, the application of systems-level and bioinformatics investigation will be a powerful strategy to identify novel precision treatment options for UM and a myriad of Gαq-driven diseases.

STAR★METHODS

CONTACT FOR REAGENT AND RESOURCE SHARING

Requests for further information or resources and reagents should be directed to and will be fulfilled by the Lead Contact, Dr. J. Silvio Gutkind (sgutkind@ucsd.edu). Plasmids used and generated in this study are subject to restrictions under a simple material transfer agreement (MTA) with UCSD.

EXPERIMENTAL MODEL AND SUBJECT DETAILS

Cell lines, culture procedures and chemicals—HEK293 and HEK293T cells were cultured in DMEM (Sigma-Aldrich Inc., MO) containing 10% FBS (Sigma-Aldrich Inc., MO) and 1× antibiotic/antimycotic solution (Sigma-Aldrich Inc., MO). Culture conditions for UM cells (OMM1.3, OMM1.5, MEL202, MEL270 and 92.1) have been described elsewhere (Schmitt et al., 2007; Zuidervaart et al., 2005). SK-MEL-28 cells were purchased

from ATCC and cultured following ATCC recommendations in EMEM containing 10% FBS. VS-4718 (PND-1186) was purchased from MedChemExpress (MCE) pre-prepared as a 10mM solution in DMSO. FR900359 (FR) was graciously supplied by the lab of Dr. Evi Kostenis.

DNA constructs—Plasmids pCEFL-HA, pCEFL-HA-GαqQL, pCEFL-HA-Gαq-DREADD, pCEFL-3x-Flag-Renilla-luciferase were described previously (Marinissen et al., 2003; Teramoto et al., 2003). pCEFL-myr-FAK was described previously (Chikumi et al., 2002; Igishi et al., 1999). Plasmids pCMV-myc-MST1 (Addgene #8847, originally from Joseph Avruch's lab), pCMV2-FLAG-SAV1 (Addgene #18970, originally from Marius Sudol' lab), pcDNA3-HA-MOB1 (Addgene #32835, originally from Kunliang Guan's lab), p2xFLAG-CMV2-LATS1 (Addgene #18971, originally from Marius Sudol's lab) and 8xGTIIC-luciferase (Addgene #34615, originally from Stefano Piccolo's Lab).

METHOD DETAILS

Bioinformatic analysis (Identifying clinically-relevant Gαq-specific vulnerabilities of UM): To identify the *clinically-relevant* vulnerabilities for UM, we performed an analysis that follows the main concepts of our previous work, ISLE (Lee et al., 2018) with modifications for Gαq-driven UM. We analyzed the cancer genome atlas (TCGA) (Cancer Genome Atlas Research et al., 2013) UM samples with skin cutaneous melanoma (SKCM) samples as control together with the large-scale functional (Cheung et al., 2011; Cowley et al., 2014; Marcotte et al., 2012; Marcotte et al., 2016) and drug response (Barretina et al., 2012; Friedman et al., 2015; Iorio et al., 2016) screens. We downloaded the gene expression, copy number alteration, and patient survival and other clinical characteristics of TCGA UM and SKCM cohort from cBioPortal (Gao et al., 2013) on Feb 1, 2017. We used 80 UM samples and 287 SKCM samples for our analysis. We obtained the data from cBioPortal as it integrates the mutation analysis from different TCGA centers to avoid center specific bias in mutation calls.

We denoted a tumor sample as Gαq+ if any of the Gαq-family genes *(GNAQ, GNA11* and *CYSLTR2*) are either mutated or amplified in the given sample (amplification, if the Gistic score is greater than 0.35), and as Gαq-if the sample lacks *GNAQ, GNA11* and *CYSLTR2* genes mutation and amplification. First, we selected important genes in UM, that are (i) highly over expressed in Gαq+ UM (n=77, excluding 3 Gαq-cases) with respect to control Gαq-SKCM TCGA samples (n=209) using Wilcoxon rank sum test ($p<0.05$). We filtered out (ii) those genes that are overexpressed in UM compared to all SKCM samples irrespective of Gαq status (Wilcoxon rank sum $p>0.05$), leading to 1,146 out of total 18,087 satisfying both conditions. We tested whether these genes show significant overlap with the genes overexpressed in Gαq+ skin melanoma TCGA samples (n=78, mutation=16, amplification=65, overlap=13) compared to Gαq-SKCM samples using hypergeometric test, truncating the hypergeometric p values to 10^{-16}.

Second, we further selected the genes whose inactivation leads to better patient survival in UM, thus potential target of a therapy. We used a stratified Cox proportional hazard model to evaluate the association, while controlling for available potential confounders in the dataset

including patients' sex and tumor stage (Therneau and Grambsch, 2000). The inactivation of 293 genes (out of 1,146 genes that passed the previous screen) show significant association with improved patient survival.

Third, we used gene essentiality (Cheung et al., 2011; Cowley et al., 2014; Marcotte et al., 2012; Marcotte et al., 2016) and drug response screens (Barretina et al., 2012; Friedman et al., 2015; Iorio et al., 2016) in a wide panel of cancer cell lines to identify the genes whose knockdown/inhibition specifically reduces Gαq+ cell viability. We used the mutation and copy number data from the measurements on the cell lines in CCLE collection (Barretina et al., 2012) to determine the status of Gαq-family genes in these cell lines. We performed Wilcoxon rank sum test between the essentiality or drug response values between the cell lines that are Gαq+ *vs.* Gαq-. The essentiality or the drug inhibition identified 72 genes out of 293 genes (that passed the 2nd filter) that satisfy this condition.

Finally, we prioritized the druggable targets. We collected the druggable genome using the drug-to-target mapping curated in DrugBank database (Law et al., 2014) and the literature including (Barretina et al., 2012; Basu et al., 2013; Friedman et al., 2015; Gao et al., 2013; Garnett et al., 2012; Iorio et al., 2016). Our collection encompasses 756 targetable genes, including 273 targets of FDA-approved drugs, 10 targets of drugs under clinical trials, and 473 experimental drugs. We further removed the genes that belong to the same chromosomes to the Gαq-family genes to avoid the confounding effect of genomic linkage. This step led to the final set of 7 targets.

Immunoblot assay—Western blot assays were performed as described previously (Feng et al., 2014b). Western blots were developed using Immobilon Western Chemiluminescent HRP substrate (Millipore, MA) according to the manufacturer's instructions.

CRISPR-Cas9-knockout—*PTK2*-sgRNA-CRISPR/Cas9-all-in-one-lentivector vector was purchased from Applied Biological Materials Inc. (Cat. K1752206). Lentivirus were prepared with HEK293T cells as the packaging cells as previously reported (Basile et al., 2004). To establish *PTK2*-knock out, cells were infected with the corresponding lentiviral supernatants for 16 hours, after which the media was changed to normal growth medium containing puromycin (Sigma-Aldrich Inc., MO) selection.

siRNAs transfection—All cells were transfected using Lipofectamine® RNAiMAX Reagent (Thermo Fisher Scientific) according to manufacturer's instructions.

MOB1-Y26F point mutation—MOB1-Y26F point mutant was generated using the Quickchange Site-Directed Mutagenesis kit following manufacturer's instructions (Agilent Genomics, CA). pcDNA3-HA-MOB1 was used as the template and the primers were designed as follows. Y26F-forward: 5'- CAT GTTTT AAGAGTT CAAACT GATGAGATCCTT CAGGGAT ATT CTT C-3', Y26F-reverse: 5'-GAAGAAT ATCCCTGAAGGAT CT CAT CAGTTTGAACT CTT AAAACATG-3'.

Human tumors xenografts and VS-4718 in vivo treatment—Female NOD.Cg-Prkdcscid Il2rgtm1wjl/SzJ mice (commonly known as NOD scid gamma, Jackson

Laboratory, Maine), 6 to 8 weeks of age and weighing 18 to 20g, were used in the study of UM cells, housed in appropriate sterile filter-capped cages, and provided food and water ad libitum. All procedures were essentially as previously described (Feng et al., 2014b; Schrage et al., 2015; Vaque et al., 2013). Briefly, exponentially growing cultures were harvested, washed, resuspended in RPMI 1640, and 2×10^6 viable cells were transplanted subcutaneously into the flanks of mice. For tumor growth analysis, tumor volume was assessed as [($LW^2/2$); where L and W represent the length and the width of the tumor]. The animals were monitored twice weekly for tumor development. Results of animal experiments were expressed as mean ± SEM of a total of tumors analyzed. To administer VS-4718 (Verastem Oncology; Needham, MA) to mice, 10mg/ml VS-4718 was prepared in 0.5% carboxymethyl cellulose (CMC) (C5678, Sigma-Aldrich; St . Louis, MO) 0.1% Tween 80 (P1754, Sigma Aldrich; St. Louis, MO) in sterile water, 100 mg/kg administered via oral gavage twice daily, control group was treated with vehicle.

Immunofluorescence—Cells cultured on coverslips were washed with PBS, fixed with 3.7% formaldehyde in phosphate-buffered saline (PBS) for 30 min, and permeabilized using 0.05% Triton X-100 for 10 min. Fixed cells were blocked with 3% FBS-containing PBS for 30 min, and incubated with YAP (Cell signaling technology, MI) antibody (in 3% FBS-PBS otherwise stated) for 1h at room temperature.

The reaction was visualized with Alexa-labeled secondary antibodies (Invitrogen, CA). Samples were mounted in PBS buffer containing Hoechst 33342 (Molecular Probes, OR) for nuclear staining. Images were acquired with an Axio Imager Z1 microscope equipped with ApoTome system controlled by ZEN 2012 software (Carl Zeiss, NY).

Luciferase assays—Cells were co-transfected with pCEFL-3x-Flag-Renilla-luciferase and 8xGTIIC-luciferase (Addgene 34615) in 6-well plates overnight to the detection of the luciferase activity, using a Dual-Glo Luciferase Assay Kit (Promega, WI) and a Microtiter plate luminometer (Dynex Tech., VA).

Immunohistochemistry—The following antibodies were used for immunohistochemistry anti-Ki67 (DAKO) and anti-YAP (CST). Unstained 5μm paraffin sections were dewaxed in Safeclear II (Fisher Scientific, PA), hydrated through graded alcohols and distilled water, and washed three times with PBS. Antigens were retrieved using or 10mM citrate buffer boiled in a microwave for 20 min (2 min at 100% power and 18 min at 10% power). The slides were allowed to cool down for 30 min at room temperature, rinsed twice with PBS, incubated in 3% hydrogen peroxide in PBS for 10 min to quench the endogenous peroxidase. The sections were then sequentially washed in distilled water and PBS, incubated in blocking solution (2.5% bovine serum albumin in PBS) for 30 min at room temperature. Excess solution was discarded and the primary antibodies were applied diluted in blocking solution at 4°C overnight. After washing with PBS, the slides were sequentially incubated with the biotinylated secondary antibody (1:400) (Vector Laboratories, CA) for 30 min and with the avidin-biotin complex, reconstituted according to the instruction of the manufacturer in PBS (Vector Stain Elite, ABC kit) (Vector Laboratories, CA), for 30 min at room temperature. The slides were developed in 3,3-diaminobenzidine (Sigma FASTDAB tablet) (Sigma Chemical, MO) diluted in distilled water under a microscope.

Immunoprecipitation—Cells were lysed with IP lysis buffer [10mM Tris-Cl (pH 8.0), 150mM NaCl, 1mM EDTA, 0.3% CHAPS, 50mM NaF, 1.5mM Na3VO4, protease inhibitor (Thermo Scientific, CO), 1mM DTT, 1mM PMSF], and centrifuged at 16,000g for 5min at 4°C. Supernatants were incubated with first antibody for 1h at 4°C, and protein G or protein A conjugated resin for another 1h. Resins were then washed 3 times with lysis buffer and boiled in SDS-loading buffer.

Cell growth assays—Cell growth assays were performed as described previously (Yamaguchi et al., 2016). Cells were cultured in 96-well-plate and treated with drugs for 72 hours. The manufacturer's instructions of Alamar Blue Cell Viability Reagent were followed to complete the assay.

3D cell culture—3-dimensional cultures were performed as described previously (Tancioni et al., 2015). Briefly, 10,000 cells were embedded in 1% methylcellulose diluted in growth media and plated onto 6-well poly-hyodroxyethyl methacrylic acid (poly-HEMA)-coated plates.

Generation of GST-MOB fusion proteins—GST fusion proteins were prepared engineered, expressed in bacteria, and purified as previously described in (Martin et al., 2018) using standard procedures.

In vitro FAK kinase assay—Kinase reactions were performed as previously described in Bernard-Trifilo et al. Briefly, 1.5 μg of substrate (MOB1-GST, MOB1-Y26F-GST, GST-only control, or recombinant YAP) was resuspended in 40uL FAK Kinase buffer (20mM HEPES pH 7.4, 10% glycerol, 10mM $MgCl_2$, 10mM $MnCl_2$, and 150mM NaCl). 5μL magnesium/ATP cocktail (75mM $MgCl_2$, 20mM MOPS pH 7.2, 25mM β-glycerol phosphate, 5mM EGTA, 1mM sodium orthovanadate, 1mM dithiothreitol) with or without 50μM ATP was added to appropriate tubes, and placed in 32° water bath for 15 minutes. Samples were bolied in sample buffer and processed on SDS-PAGE.

Nuclear and Cytoplasm Extraction—Subcellular fractionated lysates were generated using NE-PER Nuclear and Cytoplasmic Extraction Reagents (Thermo Scientific, CO) following manufacturer instructions.

Statistical analysis—All data analysis was performed using GraphPad Prism version 7.03 for Windows (GraphPad Software, CA). The data were analyzed by ANOVA test or t-test (* $p<0.05$, ** $p<0.01$, *** $p< 0.001$).

Supplementary Material

Refer to Web version on PubMed Central for supplementary material.

ACKNOWLEDGMENTS

We thank Monica Acosta, James Nguyen and Dana J. Steffen for their kind help and advice with some of the experiments. This work was supported by grants R33CA225291 (J.S.G, J.S.L., and E.R.), U01CA217885 (P.Y., J.S.G. and H.Y.), P30 CA023100 (P.T. and H.Y.), R01HG009285 (P.T.), NIH10193SC (P.T.), CA209891 (P.T., J.S.G. and X.F.), CA102310 (D.D.S), T32GM007752 (N.A.), DGE-1650112 (N.A.), T32CA067754–22 (A.K.), 111

Project of MOE (B14038) China (Q.C. and X.F.), the National Natural Science Foundation (81672677) China (X.F.) and Associazione Italiana per la Ricerca sul Cancro (AIRC, IG 21322) Italy (M.M and D.C.R).

REFERENCES

Armbruster BN, Li X, Pausch MH, Herlitze S, and Roth BL (2007). Evolving the lock to fit the key to create a family of G protein-coupled receptors potently activated by an inert ligand. Proc Natl Acad Sci U S A 104, 5163–5168. [PubMed: 17360345]

Arnold JJ, Blinder KJ, Bressler NM, Bressler SB, Burdan A, Haynes L, Lim JI, Miller JW, Potter MJ, Reaves A, et al. (2004). Acute severe visual acuity decrease after photodynamic therapy with verteporfin: case reports from randomized clinical trials-TAP and VIP report no. 3. Am J Ophthalmol 137, 683–696. [PubMed: 15059708]

Azab M, Benchaboune M, Blinder KJ, Bressler NM, Bressler SB, Gragoudas ES, Fish GE, Hao Y, Haynes L, Lim JI, et al. (2004). Verteporfin therapy of subfoveal choroidal neovascularization in age-related macular degeneration: meta-analysis of 2-year safety results in three randomized clinical trials: Treatment Of Age-Related Macular Degeneration With Photodynamic Therapy and Verteporfin In Photodynamic Therapy Study Report no. 4. Retina 24, 1–12. [PubMed: 15076937]

Barbazetto IA, Lee TC, Rollins IS, Chang S, and Abramson DH (2003). Treatment of choroidal melanoma using photodynamic therapy. Am J Ophthalmol 135, 898–899. [PubMed: 12788137]

Barretina J, Caponigro G, Stransky N, Venkatesan K, Margolin AA, Kim S, Wilson CJ, Lehar J, Kryukov GV, Sonkin D, et al. (2012). The Cancer Cell Line Encyclopedia enables predictive modelling of anticancer drug sensitivity. Nature 483, 603–607. [PubMed: 22460905]

Basu A, Bodycombe NE, Cheah JH, Price EV, Liu K, Schaefer GI, Ebright RY, Stewart ML, Ito D, Wang S, et al. (2013). An Interactive Resource to Identify Cancer Genetic and Lineage Dependencies Targeted by Small Molecules. Cell 154, 1151–1161. [PubMed: 23993102]

Bhatt M, Shah S, and Shivprakash (2010). Development of a high-throughput method for the determination of ethosuximide in human plasma by liquid chromatography mass spectrometry. J Chromatogr B Analyt Technol Biomed Life Sci 878, 1605–1610.

Cancer Genome Atlas Research, N., Weinstein JN, Collisson EA, Mills GB, Shaw KR, Ozenberger BA, Ellrott K, Shmulevich I, Sander C, and Stuart JM (2013). The Cancer Genome Atlas Pan-Cancer analysis project. Nat Genet 45, 1113–1120. [PubMed: 24071849]

Carvajal RD, Piperno-Neumann S, Kapiteijn E, Chapman PB, Frank S, Joshua AM, Piulats JM, Wolter P, Cocquyt V, Chmielowski B, et al. (2018). Selumetinib in Combination With Dacarbazine in Patients With Metastatic Uveal Melanoma: A Phase III, Multicenter, Randomized Trial (SUMIT). J Clin Oncol 36, 1232–1239. [PubMed: 29528792]

Carvajal RD, Sosman JA, Quevedo JF, Milhem MM, Joshua AM, Kudchadkar RR, Linette GP, Gajewski TF, Lutzky J, Lawson DH, et al. (2014). Effect of selumetinib vs chemotherapy on progression-free survival in uveal melanoma: a randomized clinical trial. Jama 311, 2397–2405. [PubMed: 24938562]

Chen X, Wu Q, Depeille P, Chen P, Thornton S, Kalirai H, Coupland SE, Roose JP, and Bastian BC (2017). RasGRP3 Mediates MAPK Pathway Activation in GnAQ Mutant Uveal Melanoma. Cancer Cell 31, 685–696 e686. [PubMed: 28486107]

Cheung HW, Cowley GS, Weir BA, Boehm JS, Rusin S, Scott JA, East A, Ali LD, Lizotte PH, Wong TC, et al. (2011). Systematic investigation of genetic vulnerabilities across cancer cell lines reveals lineage-specific dependencies in ovarian cancer. Proceedings of the National Academy of Sciences of the United States of America 108, 12372–12377. [PubMed: 21746896]

Chikumi H, Fukuhara S, and Gutkind JS (2002). Regulation of G protein-linked guanine nucleotide exchange factors for Rho, PDZ-RhoGEF, and LARG by tyrosine phosphorylation: evidence of a role for focal adhesion kinase. J Biol Chem 277, 12463–12473. [PubMed: 11799111]

Cowley GS, Weir BA, Vazquez F, Tamayo P, Scott JA, Rusin S, East-Seletsky A, Ali LD, Gerath WF, Pantel SE, et al. (2014). Parallel genome-scale loss of function screens in 216 cancer cell lines for the identification of context-specific genetic dependencies. Sci Data 1, 140035.

Dorsam RT, and Gutkind JS (2007). G-protein-coupled receptors and cancer. Nat Rev Cancer 7, 79–94. [PubMed: 17251915]

Feng X, Chen Q, and Gutkind JS (2014a). Oncotargeting G proteins: The Hippo in the room. Oncotarget 5, 10997–10999. [PubMed: 25526026]

Feng X, Degese MS, Iglesias-Bartolome R, Vaque JP, Molinolo AA, Rodrigues M, Zaidi MR, Ksander BR, Merlino G, Sodhi A, et al. (2014b). Hippo-independent activation of YAP by the GNAQ uveal melanoma oncogene through a trio-regulated rho GTPase signaling circuitry. Cancer Cell 25, 831–845. [PubMed: 24882515]

Friedman AA, Amzallag A, Pruteanu-Malinici I, Baniya S, Cooper ZA, Piris A, Hargreaves L, Igras V, Frederick DT, Lawrence DP, et al. (2015). Landscape of Targeted Anti-Cancer Drug Synergies in Melanoma Identifies a Novel BRAF- VEGFR/PDGFR Combination Treatment. PLoS One 10, e0140310.

Gao J, Aksoy BA, Dogrusoz U, Dresdner G, Gross B, Sumer SO, Sun Y, Jacobsen A, Sinha R, Larsson E, et al. (2013). Integrative analysis of complex cancer genomics and clinical profiles using the cBioPortal. Sci Signal 6, pl1.

Garnett MJ, Edelman EJ, Heidorn SJ, Greenman CD, Dastur A, Lau KW, Greninger P, Thompson IR, Luo X, Soares J, et al. (2012). Systematic identification of genomic markers of drug sensitivity in cancer cells. Nature 483, 570-U587.

Griner EM, and Kazanietz MG (2007). Protein kinase C and other diacylglycerol effectors in cancer. Nat Rev Cancer 7, 281–294. [PubMed: 17384583]

Gutkind JS, Novotny EA, Brann MR, and Robbins KC (1991). Muscarinic acetylcholine receptor subtypes as agonist-dependent oncogenes. Proc Natl Acad Sci U S A 88, 4703–4707. [PubMed: 1905013]

Gutkind JS, and Robbins KC (1992). Activation of transforming G protein-coupled receptors induces rapid tyrosine phosphorylation of cellular proteins, including p125FAK and the p130 v-src substrate. Biochem Biophys Res Commun 188, 155–161. [PubMed: 1329743]

Howe AK (2011). Cross-talk between calcium and protein kinase A in the regulation of cell migration. Current opinion in cell biology 23, 554–561. [PubMed: 21665456]

Hu JK, Du W, Shelton SJ, Oldham MC, DiPersio CM, and Klein OD (2017). An FAK-YAP-mTOR Signaling Axis Regulates Stem Cell-Based Tissue Renewal in Mice. Cell Stem Cell 21, 91–106 e106. [PubMed: 28457749]

Hubbard KB, and Hepler JR (2006). Cell signalling diversity of the Gqalpha family of heterotrimeric G proteins. Cell Signal 18, 135–150. [PubMed: 16182515]

Igishi T, Fukuhara S, Patel V, Katz BZ, Yamada KM, and Gutkind JS (1999). Divergent signaling pathways link focal adhesion kinase to mitogen-activated protein kinase cascades. Evidence for a role of paxillin in c-Jun NH(2)-terminal kinase activation. J Biol Chem 274, 30738–30746. [PubMed: 10521463]

Ikeda F, Terajima H, Shimahara Y, Kondo T, and Yamaoka Y (2003). Reduction of hepatic ischemia/reperfusion-induced injury by a specific ROCK/Rho kinase inhibitor Y-27632. J Surg Res 109, 155–160. [PubMed: 12643858]

Iorio F, Knijnenburg TA, Vis DJ, Bignell GR, Menden MP, Schubert M, Aben N, Goncalves E, Barthorpe S, Lightfoot H, et al. (2016). A Landscape of Pharmacogenomic Interactions in Cancer. Cell 166, 740–754. [PubMed: 27397505]

Julius D, and Nathans J (2012). Signaling by sensory receptors. Cold Spring Harbor perspectives in biology 4, a005991.

Kalinec G, Nazarali AJ, Hermouet S, Xu N, and Gutkind JS (1992). Mutated alpha subunit of the Gq protein induces malignant transformation in NIH 3T3 cells. Mol Cell Biol 12, 4687–4693. [PubMed: 1328859]

Kovacs M, Toth J, Hetenyi C, Malnasi-Csizmadia A, and Sellers JR (2004). Mechanism of blebbistatin inhibition of myosin II. J Biol Chem 279, 35557–35563. [PubMed: 15205456]

Lachowski D, Cortes E, Robinson B, Rice A, Rombouts K, and Del Rio Hernandez AE (2018). FAK controls the mechanical activation of YAP, a transcriptional regulator required for durotaxis. FASEB J 32, 1099–1107. [PubMed: 29070586]

Law V, Knox C, Djoumbou Y, Jewison T, Guo AC, Liu Y, Maciejewski A, Arndt D, Wilson M, Neveu V, et al. (2014). DrugBank 4.0: shedding new light on drug metabolism. Nucleic Acids Res 42, D1091–1097.

Lee JS, Das A, Jerby-Arnon L, Arafeh R, Auslander N, Davidson M, McGarry L, James D, Amzallag A, Park SG, et al. (2018). Harnessing synthetic lethality to predict the response to cancer treatment. Nat Commun 9, 2546. [PubMed: 29959327]

Li P, Silvis MR, Honaker Y, Lien WH, Arron ST, and Vasioukhin V (2016). alphaE-catenin inhibits a Src-YAP1 oncogenic module that couples tyrosine kinases and the effector of Hippo signaling pathway. Genes Dev 30, 798–811. [PubMed: 27013234]

Liberzon A, Birger C, Thorvaldsdottir H, Ghandi M, Mesirov JP, and Tamayo P (2015). The Molecular Signatures Database (MSigDB) hallmark gene set collection. Cell systems 1, 417–425. [PubMed: 26771021]

Marcotte R, Brown KR, Suarez F, Sayad A, Karamboulas K, Krzyzanowski PM, Sircoulomb F, Medrano M, Fedyshyn Y, Koh JL, et al. (2012). Essential gene profiles in breast, pancreatic, and ovarian cancer cells. Cancer Discov 2, 172–189. [PubMed: 22585861]

Marcotte R, Sayad A, Brown KR, Sanchez-Garcia F, Reimand J, Haider M, Virtanen C, Bradner JE, Bader GD, Mills GB, et al. (2016). Functional Genomic Landscape of Human Breast Cancer Drivers, Vulnerabilities, and Resistance. Cell 164, 293–309. [PubMed: 26771497]

Marinissen MJ, Servitja JM, Offermanns S, Simon MI, and Gutkind JS (2003). Thrombin protease-activated receptor-1 signals through Gq-and G13-initiated MAPK cascades regulating c-Jun expression to induce cell transformation. J Biol Chem 278, 46814–46825. [PubMed: 12954641]

Martin D, Degese MS, Vitale-Cross L, Iglesias-Bartolome R, Valera JLC, Wang Z, Feng X, Yeerna H, Vadmal V, Moroishi T, et al. (2018). Assembly and activation of the Hippo signalome by FAT1 tumor suppressor. Nat Commun 9, 2372. [PubMed: 29985391]

Meng Z, Moroishi T, and Guan KL (2016). Mechanisms of Hippo pathway regulation. Genes Dev 30, 1–17. [PubMed: 26728553]

Moore AR, Ceraudo E, Sher JJ, Guan Y, Shoushtari AN, Chang MT, Zhang JQ, Walczak EG, Kazmi MA, Taylor BS, et al. (2016). Recurrent activating mutations of G-protein-coupled receptor CYSLTR2 in uveal melanoma. Nature Genetics 48, 675–680. [PubMed: 27089179]

Moroishi T, Hansen CG, and Guan KL (2015). The emerging roles of YAP and TAZ in cancer. Nature reviews Cancer 15, 73–79. [PubMed: 25592648]

Narumiya S, Ishizaki T, and Uehata M (2000). Use and properties of ROCK-specific inhibitor Y-27632. Methods Enzymol 325, 273–284. [PubMed: 11036610]

Newton AC (2010). Protein kinase C: poised to signal. Am J Physiol Endocrinol Metab 298, E395–402.

O'Hayre M, Vazquez-Prado J, Kufareva I, Stawiski EW, Handel TM, Seshagiri S, and Gutkind JS (2013). The emerging mutational landscape of G proteins and G-protein-coupled receptors in cancer. Nature reviews Cancer 13, 412–424. [PubMed: 23640210]

Pan D (2010). The hippo signaling pathway in development and cancer. Dev Cell 19, 491–505. [PubMed: 20951342]

Prevarskaya N, Skryma R, and Shuba Y (2011). Calcium in tumour metastasis: new roles for known actors. Nature reviews Cancer 11, 609–618. [PubMed: 21779011]

Robertson AG, Shih J, Yau C, Gibb EA, Oba J, Mungall KL, Hess JM, Uzunangelov V, Walter V, Danilova L, et al. (2017). Integrative Analysis Identifies Four Molecular and Clinical Subsets in Uveal Melanoma. Cancer Cell 32, 204–220 e215. [PubMed: 28810145]

Rozengurt E (2007). Mitogenic signaling pathways induced by G protein-coupled receptors. J Cell Physiol 213, 589–602. [PubMed: 17786953]

Sassone-Corsi P (2012). The cyclic AMP pathway. Cold Spring Harbor perspectives in biology 4.

Schrage R, Schmitz AL, Gaffal E, Annala S, Kehraus S, Wenzel D, Bullesbach KM, Bald T, Inoue A, Shinjo Y, et al. (2015). The experimental power of FR900359 to study Gq-regulated biological processes. Nat Commun 6, 10156. [PubMed: 26658454]

Soucek P, and Cihelkova I (2006). Photodynamic therapy with verteporfin in subfoveal amelanotic choroidal melanoma (A controlled case). Neuro endocrinology letters 27, 145–148. [PubMed: 16648785]

Subramanian A, Tamayo P, Mootha VK, Mukherjee S, Ebert BL, Gillette MA, Paulovich A, Pomeroy SL, Golub TR, Lander ES, et al. (2005). Gene set enrichment analysis: a knowledge-based

approach for interpreting genome-wide expression profiles. Proceedings of the National Academy of Sciences of the United States of America 102, 15545–15550. [PubMed: 16199517]

Sulzmaier FJ, Jean C, and Schlaepfer DD (2014). FAK in cancer: mechanistic findings and clinical applications. Nat Rev Cancer 14, 598–610. [PubMed: 25098269]

Tancioni I, Miller NL, Uryu S, Lawson C, Jean C, Chen XL, Kleinschmidt EG, and Schlaepfer DD (2015). FAK activity protects nucleostemin in facilitating breast cancer spheroid and tumor growth. Breast Cancer Res 17, 47. [PubMed: 25880415]

Taniguchi K, Wu LW, Grivennikov SI, de Jong PR, Lian I, Yu FX, Wang K, Ho SB, Boland BS, Chang JT, et al. (2015). A gp130-Src-YAP module links inflammation to epithelial regeneration. Nature 519, 57–62. [PubMed: 25731159]

Teramoto H, Malek RL, Behbahani B, Castellone MD, Lee NH, and Gutkind JS (2003). Identification of H-Ras, RhoA, Rac1 and Cdc42 responsive genes. Oncogene 22, 2689–2697. [PubMed: 12730683]

Therneau TM, and Grambsch PM (2000). Modeling survival data : extending the Cox model (New York: Springer).

Tsherniak A, Vazquez F, Montgomery PG, Weir BA, Kryukov G, Cowley GS, Gill S, Harrington WF, Pantel S, Krill-Burger JM, et al. (2017). Defining a Cancer Dependency Map. Cell 170, 564–576 e516. [PubMed: 28753430]

Van Raamsdonk CD, Bezrookove V, Green G, Bauer J, Gaugler L, O'Brien JM, Simpson EM, Barsh GS, and Bastian BC (2009). Frequent somatic mutations of GNAQ in uveal melanoma and blue naevi. Nature 457, 599–602. [PubMed: 19078957]

Van Raamsdonk CD, Griewank KG, Crosby MB, Garrido MC, Vemula S, Wiesner T, Obenauf AC, Wackernagel W, Green G, Bouvier N, et al. (2010). Mutations in GNA11 in uveal melanoma. N Engl J Med 363, 2191–2199. [PubMed: 21083380]

Vaque JP, Dorsam RT, Feng X, Iglesias-Bartolome R, Forsthoefel DJ, Chen Q, Debant A, Seeger MA, Ksander BR, Teramoto H, et al. (2013). A genome-wide RNAi screen reveals a Trio-regulated Rho GTPase circuitry transducing mitogenic signals initiated by G protein-coupled receptors. Mol Cell 49, 94–108. [PubMed: 23177739]

Yamaguchi K, Iglesias-Bartolome R, Wang Z, Callejas-Valera JL, Amornphimoltham P, Molinolo AA, Cohen EE, Califano JA, Lippman SM, Luo J, et al. (2016). A synthetic-lethality RNAi screen reveals an ERK-mTOR co-targeting pro-apoptotic switch in PIK3CA+ oral cancers. Oncotarget 7, 10696–10709. [PubMed: 26882569]

Yu FX, Luo J, Mo JS, Liu G, Kim YC, Meng Z, Zhao L, Peyman G, Ouyang H, Jiang W, et al. (2014a). Mutant Gq/11 promote uveal melanoma tumorigenesis by activating YAP. Cancer Cell 25, 822–830. [PubMed: 24882516]

Yu FX, Zhang K, and Guan KL (2014b). YAP as oncotarget in uveal melanoma. Oncoscience 1, 480–481. [PubMed: 25594048]

Yu FX, Zhao B, and Guan KL (2015). Hippo Pathway in Organ Size Control, Tissue Homeostasis, and Cancer. Cell 163, 811–828. [PubMed: 26544935]

Zhao B, Ye X, Yu JD, Li L, Li WQ, Li SM, Yu JJ, Lin JD, Wang CY, Chinnaiyan AM, et al. (2008). TEAD mediates YAP-dependent gene induction and growth control. Gene Dev 22, 1962–1971. [PubMed: 18579750]

SIGNIFICANCE:

Despite the central role of Hippo/YAP-regulating mechanisms in uveal melanoma (UM), there are no clinically effective therapeutic targets. Dissection of mediators regulating Hippo/YAP-signaling could identify urgently needed therapeutic opportunities to inhibit YAP-dependent tumor growth in UM and other cancers. Coupling the power of an unbiased computational pipeline to the unique genetic landscape of UM, we uncovered a novel molecular framework regulating YAP, and identified FAK as a druggable signaling hub downstream from *GNAQ* in UM. Gαq activates tyrosine phosphorylation networks through FAK, which activates YAP by a novel mechanism suppressing the Hippo kinase cascade. A new generation of FAK inhibitors suppresses YAP activation *in vivo* and halts UM growth, exposing a signaling vulnerability that can be targeted for UM treatment.

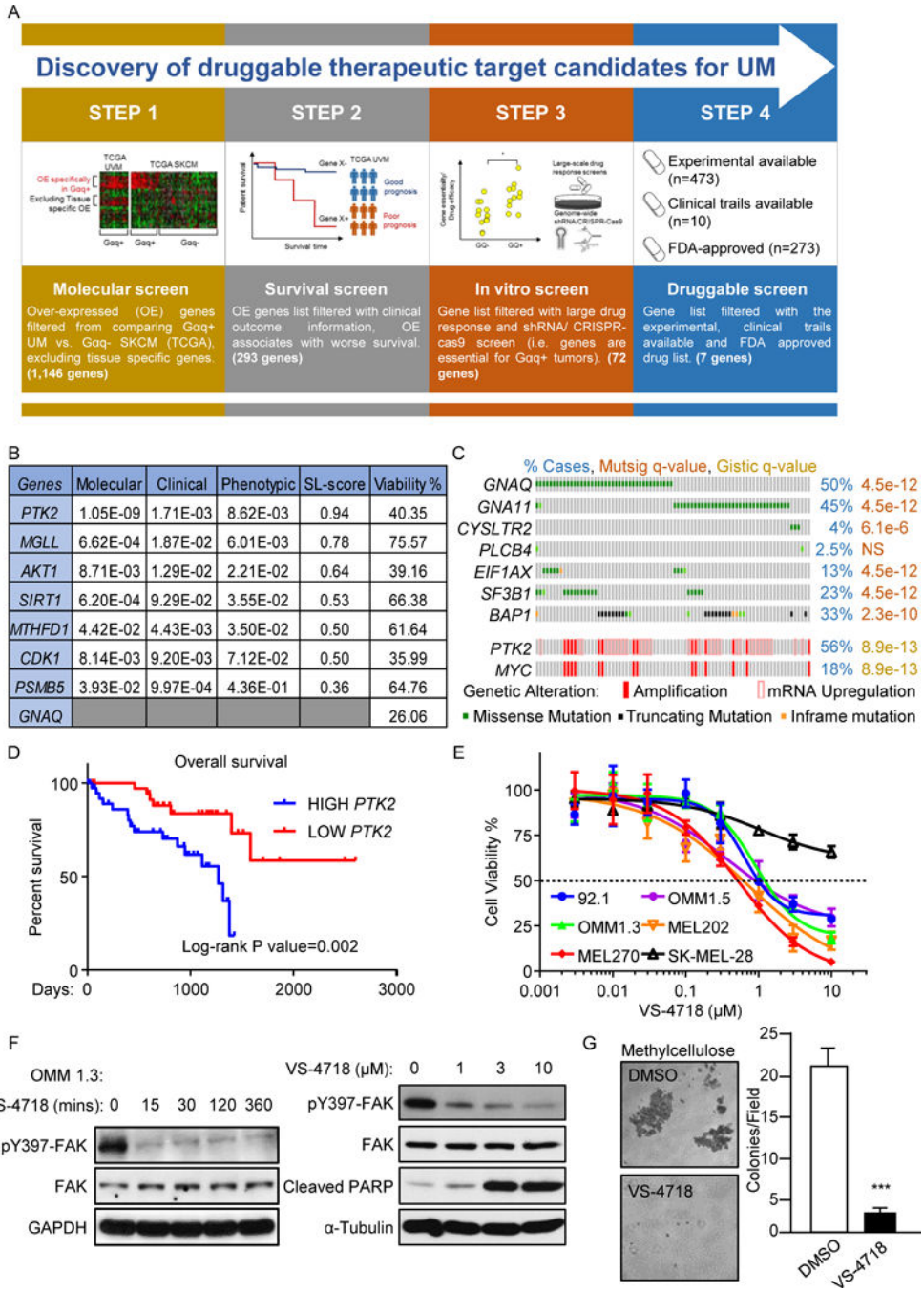

Genes	Molecular	Clinical	Phenotypic	SL-score	Viability %
PTK2	1.05E-09	1.71E-03	8.62E-03	0.94	40.35
MGLL	6.62E-04	1.87E-02	6.01E-03	0.78	75.57
AKT1	8.71E-03	1.29E-02	2.21E-02	0.64	39.16
SIRT1	6.20E-04	9.29E-02	3.55E-02	0.53	66.38
MTHFD1	4.42E-02	4.43E-03	3.50E-02	0.50	61.64
CDK1	8.14E-03	9.20E-03	7.12E-02	0.50	35.99
PSMB5	3.93E-02	9.97E-04	4.36E-01	0.36	64.76
GNAQ					26.06

Figure 1. Bioinformatics analysis reveals FAK as critical for UM progression.

A. Pipeline to identify and discover druggable therapeutic target-genes in UM: molecular screen, survival screen, in vitro screen and druggable screen. B. Table depicting the final 7 gene hits of our analysis. Molecular, clinical, phenotypic and synthetic lethal (SL) scores were calculated via our bioinformatic pipeline (Lee et al., 2018). Cell viability was assessed *in vitro* in UM cells (OMM1.3) following siRNA-mediated inhibition of each gene (cell viability normalized to OMM1.3 treated with non-targeting siRNA, siRNA-*GNAQ* used as positive control, mean, n=3). C. Oncoprint depicting the genomic landscape of TCGA uveal

melanoma patient cohort (Robertson et al., 2017). Each bar represents one patient and their respective mutation or gene expression status (data were downloaded from TCGA UM cohort from cBioPortal (Gao et al., 2013). MutSig Q value is listed on the right. D. Kaplan-Meier plot depicting overall survival for UM patients stratified against FAK expression. FAK-High and FAK-Low groups are defined as top and bottom 50% of FAK gene expression. p value=0.002. E. UM cell lines (MEL270, 92.1, OMM1.3, OMM1.5 and MEL202 with *GNAQ* active mutation) are sensitive to FAK inhibition in a dose-dependent manner after treatment with VS-4718, SKCM cells (SK-MEL-28 with *BRAF* mutation) served as control. Driver oncogenes are indicated. Data are the percent viability normalized to vehicle treatment (mean ± SEM, n=3). F. VS-4718 inhibits FAK activation in OMM1.3 (decrease in pY397- FAK, left panel) and induces apoptosis (increased cleaved PARP, right panel). G. VS-4718 inhibits OMM1.3 colony formation in semisolid media (mean ± SEM, n=3; ***, p<0.001).

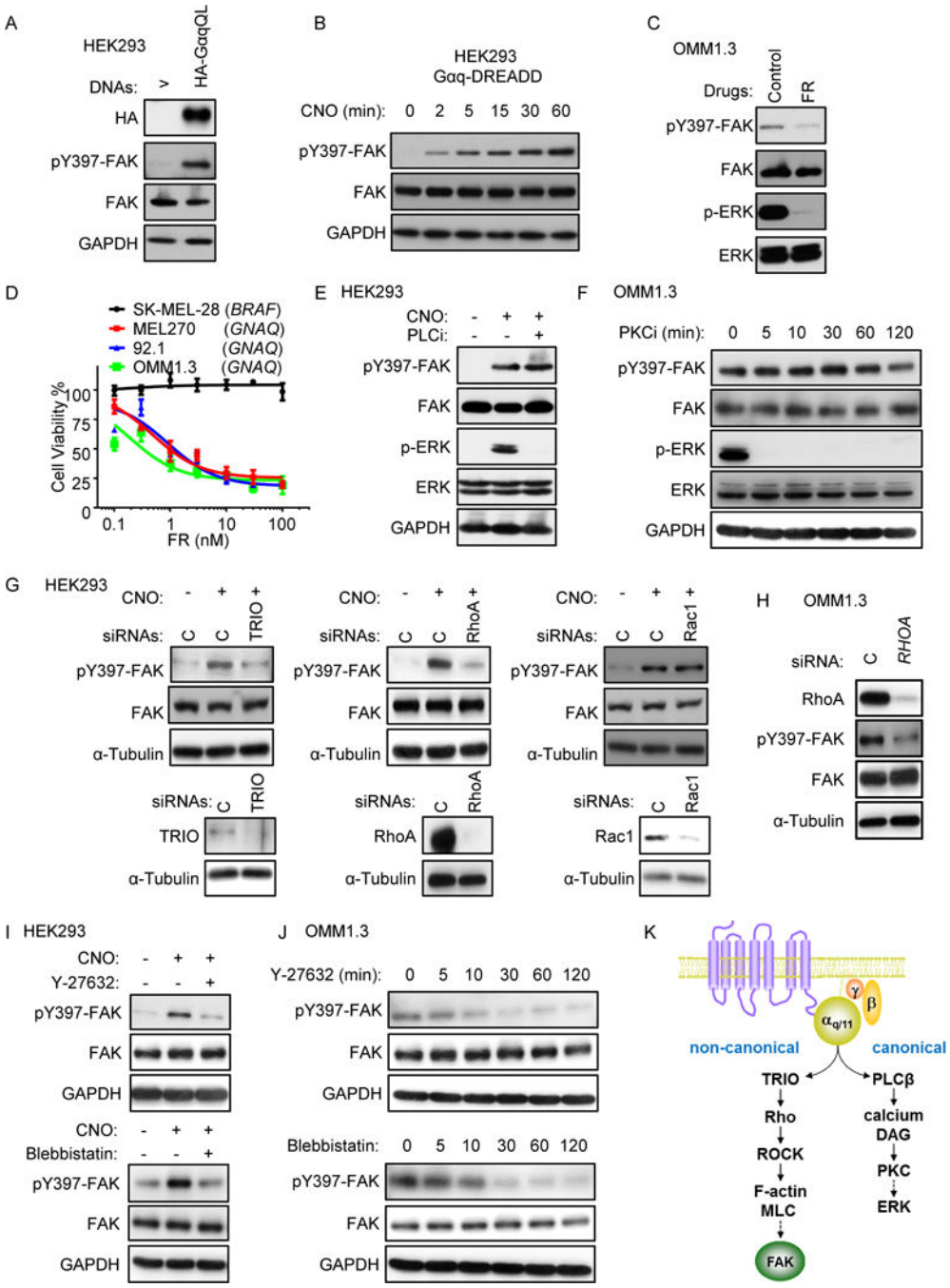

Figure 2. Gαq regulates FAK activation through a non-canonical TRIO/RhoA-mediated signaling circuitry.

A. Immunoblot depicting phosphorylation of FAK after transfection with HA-GαqQL and control expression vectors in HEK293 cells. B. Immunoblot showing FAK phosphorylation in Gαq-DREADD expressing HEK293 cells stimulated with synthetic ligand clozapine N -oxide (CNO) over a time course analysis. C. Immunoblot depicting FAK and ERK phosphorylation after FR treatment (1 μM) in OMM1.3 cells. D. UM cell lines are sensitive to Gαq inhibition in a dose-dependent manner after treatment with FR900359 (FR), SK-MEL-28 *BRAF* SKCM served as control, percent viability is normalized to vehicle

treatment (mean ± SEM, n=3). E. Immunoblot showing phosphorylation of ERK and FAK after stimulation of Gαq-DREADD expressing HEK293 cells with CNO at 5 min in combination with U73122 (1μM, PLC inhibitor) treatment. F. Immunoblot showing phosphorylation of ERK and FAK during a time course of treatment with GF109203X (1μM, PKC inhibitor) in OMM1.3 cells. G. Immunoblot showing FAK phosphorylation in Gαq-DREADD expressing HEK293 cells after 5 min of CNO stimulation in combination with siRNA mediated *TRIO, RHOA* or *RAC1* knockdown (upper panel), and immunoblot to show efficiency of siRNA mediated *TRIO, RHOA* or *RAC1* knockdown (lower panel). H. Immunoblot showing FAK phosphorylation after siRNA mediated *RHOA* knockdown in OMM1.3 cells. I. Immunoblot showing FAK phosphorylation in Gαq-DREADD expressing HEK293 cells after 5 min of CNO stimulation in combination with Y-27632 (10μM) treatment (upper panel), and in combination with blebbistatin (20μM) treatment (lower panel). J. Immunoblot showing FAK phosphorylation during a time course of treatment with Y-27632 (upper panel) and blebbistatin (lower panel) in OMM1.3 cells. K. Cartoon depicting the non-canonical signaling pathway regulating FAK activation by Gαq.

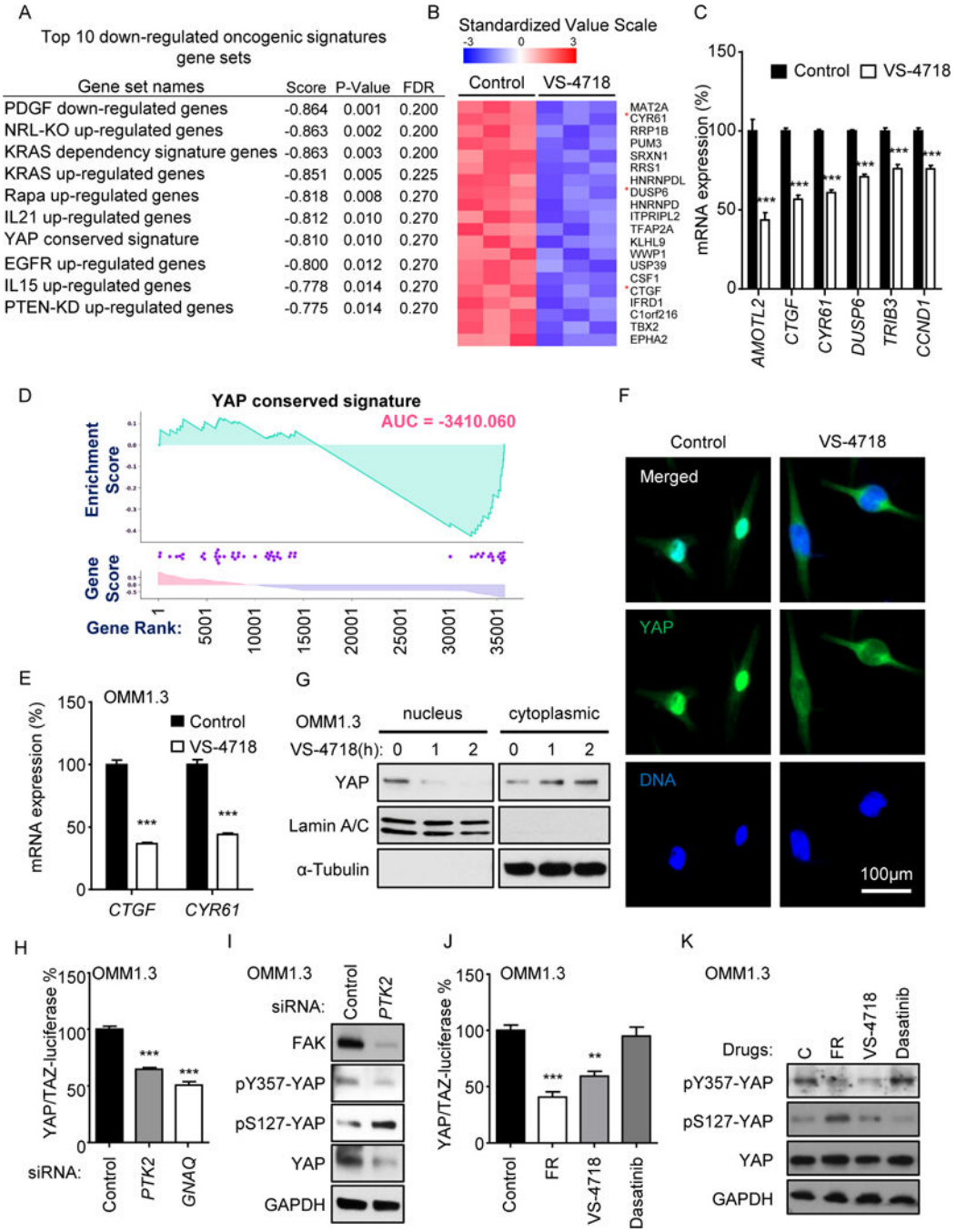

Figure 3. FAK inhibition regulates the Hippo-YAP pathway in UM.

A. The top 10 down-regulated oncogenic signatures gene sets from RNA-seq analysis of OMM1.3 cells treated with VS-4718 (1μM, vehicle treatment as control). B. Heatmap depicting the most down-regulated genes by VS-4718 treatment (as A), *=YAP signature genes. C. mRNA expression level of YAP signature genes from RNA-seq data (mean ± SEM, n=3). D. Enrichment plot for YAP Conserved Signature gene set (GSEA, http://software.broadinstitute.org/gsea/index.jsp). E. mRNA expression of *CTGF* and *CYR61* measured by qPCR in UM cells OMM1.3 with VS-4718 treatment (1μM, vehicle treatment

as control, mean ± SEM, n=3). F. Immunofluorescent staining of endogenous YAP (green) and Hoeschst staining for nuclear DNA (blue) in OMM1.3 cells after VS-4718 treatment (1μM, vehicle treatment as control). G. Immunoblot showing YAP nuclear and cytoplasmic localization after VS-4718 (1μM) treatment, using enrichment in lamin A/C and α-tubulin as nuclear and cytoplasmic markers, respectively. H. YAP/TAZ Luciferase reporter assay measuring YAP activity after siRNA mediated *PTK2* and *GNAQ* knockdown in OMM1.3 cells (mean ± SEM, n=3). I. Immunoblot showing YAP phosphorylation after siRNA mediated *PTK2* knockdown in OMM1.3 cells. J. YAP/TAZ Luciferase reporter assay measuring YAP activity after treatment with FR900359 (FR), VS-4718 or Dasatinib (1μM) in OMM1.3 cells (mean ± SEM, n=3). K. Immunoblot showing YAP phosphorylation after FR900359 (FR), VS-4718 or Dasatinib (1μM) treatment in OMM1.3 cells. (In all cases, **, $p<0.01$; ***, $p<0.001$).

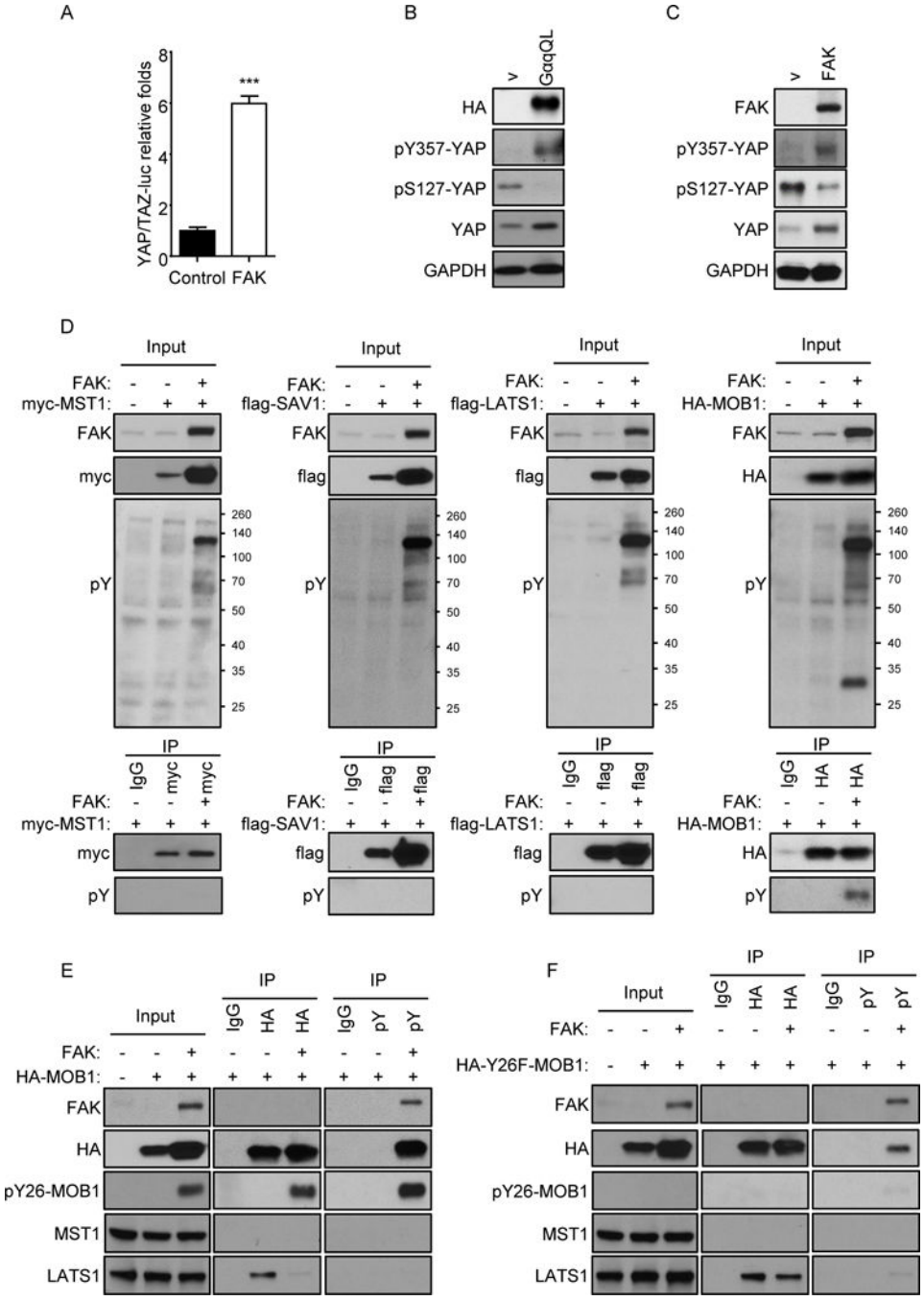

Figure 4. FAK regulates YAP activation through MOB-Y26 phosphorylation, disrupting the core Hippo kinase signaling pathway.

A. Fold-change induction of YAP activity measured by YAP/TAZ Luciferase reporter assay after transient transfection of FAK and control expression vectors in HEK293 cells (mean ± SEM, n=3; ***, p<0.001). B. Immunoblot showing phosphorylation status of YAP after transfection of HA-GαqQL and control expression vectors in HEK293 cells. C. Immunoblot showing phosphorylation status of YAP after transfection of FAK and control expression vectors in HEK293 cells. D. Immunoblot against phospho-tyrosine after immunoprecipitation (IP) of tagged Hippo signaling core components (myc-MST1, flag-

SAV1, flag-LATS1 or HA-MOB1) transfected with or without FAK in HEK293 cells. Total cell lysates (input) and IP by the indicated antibodies are shown. Western blot for FAK and each of the epitope tags are also shown. E. Immunoblot showing phosphorylation of MOB1 and association with Mst1 and LATS1 after HA or pY immunoprecipitation (IP) in HEK293 cells transfected with or without FAK and wildtype HA-MOB1. F. Immunoblot showing phosphorylation of MOB1 and association with MST1 and LATS1 after HA or pY immunoprecipitation in HEK293 cells transfected with or without FAK and mutant HA-Y26F-MOB1-.

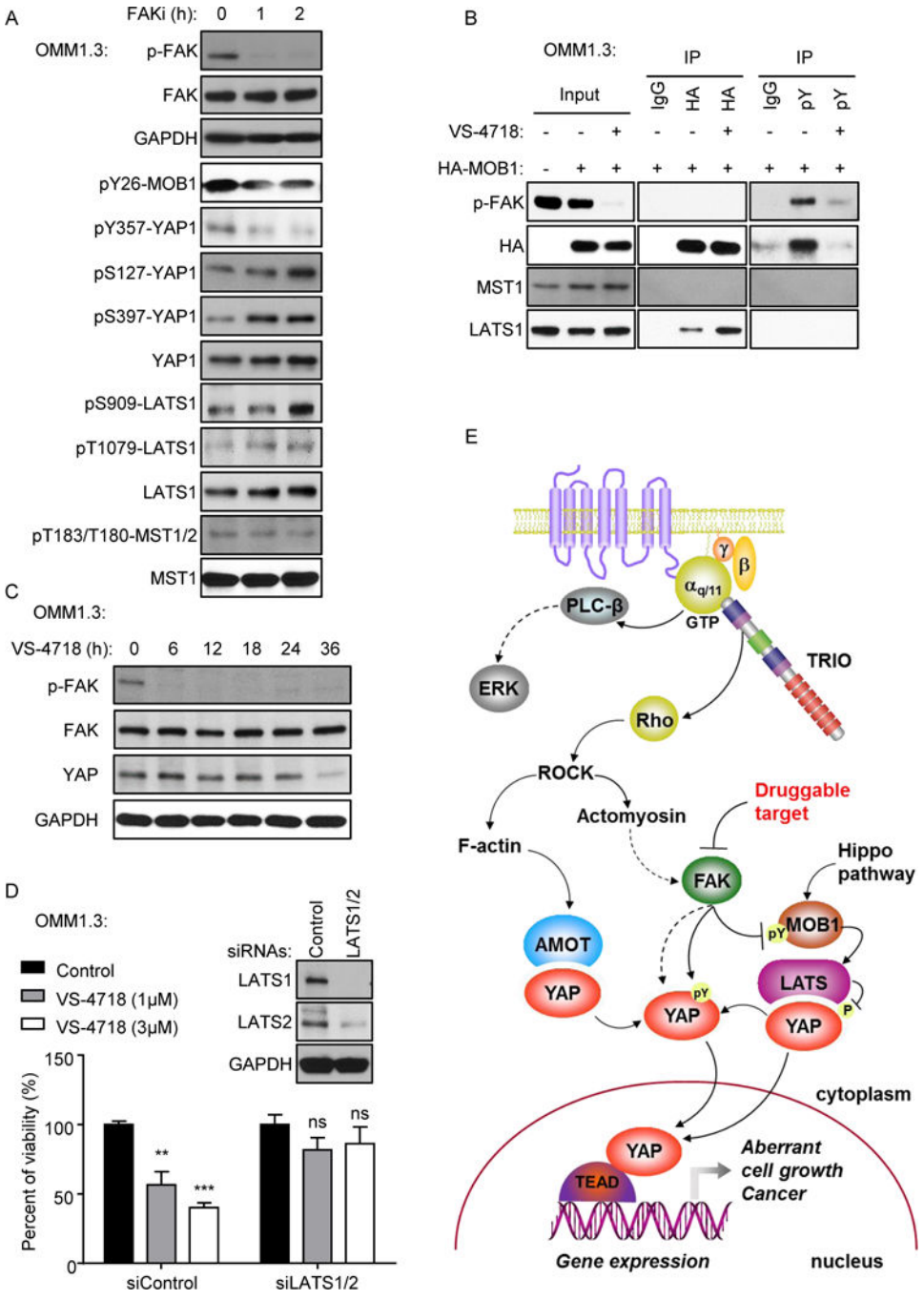

Figure 5. Inhibition of FAK causes YAP inhibition in UM by unleashing Hippo pathway signaling, and inducing inhibitory YAP phosphorylation and degradation.

A. Immunoblot of total and phosphorylated core Hippo pathway members in OMM1.3 cells after VS-4718 treatment (1μM) for 0, 1 and 2 hours. B. Immunoblot showing the reassociation of MOB1 with LATS1 after HA or pY immunoprecipitation of OMM1.3 cells transfected with HA-MOB1 with or without treatment with VS-4718. C. Immunoblot showing levels of total YAP over a time course of VS-4718 treatment (1μM) in OMM1.3 cells. D. Knockdown of LATS1/2 in OMM1.3 cells rescues from the effect of VS-4718 treatment measured by cell viability assay (lower panel, mean ± SEM, n=3; **, p<0.01, ***,

p<0.001, ns; not significant). Immunoblot showing LATS1/2 knockdown in OMM1.3 (upper panel). E. Cartoon depicting the signaling pathway by which FAK mediates YAP activation downstream from constitutively active Gαq mutant in UM. See text for details.

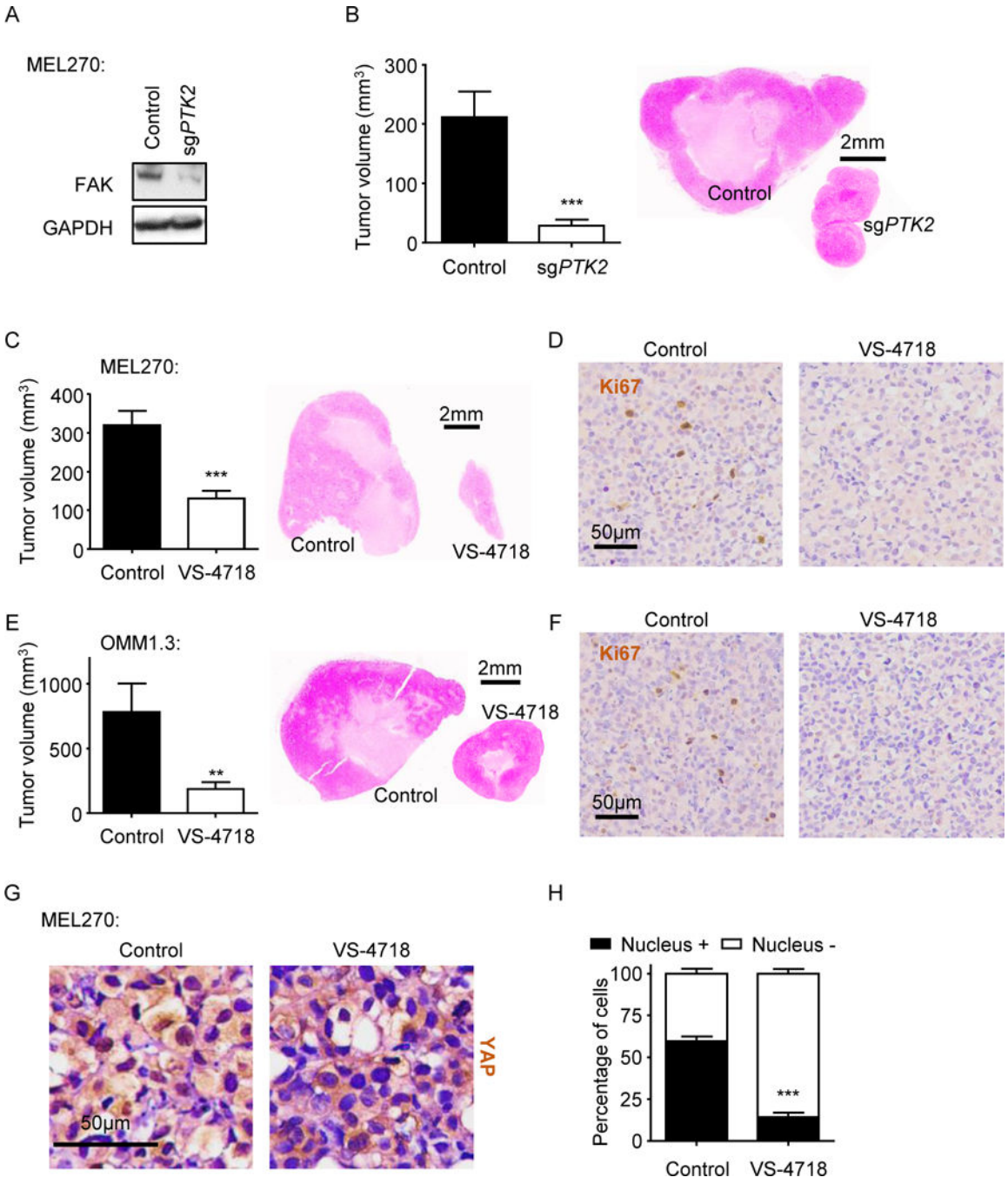

Fig 6. FAKi in UM inhibits YAP-dependent UM tumor growth.

A. Immunoblot showing CRISPR/Cas9-mediated *PTK2* knockout in MEL270 cells (wildtype as control). B. Tumor formation *in vivo* is significantly impacted in MEL270 cells with CRISPR/Cas9-mediated *PTK2* knockout (wildtype as control), tumor size at the end of the study were measured (mean ± SEM, n=4) (left panel), and hematoxylin and eosin (H&E)-stained sections of representative tumors from each group are shown (right panel). C. Tumor volume of MEL270 cells *in vivo* with or without VS-4718 treatment, tumor size at the end of the study were measured (mean ± SEM, n=8) (left panel), and hematoxylin and

eosin (H&E)-stained sections of representative tumors from each group are shown (right panel). D. Ki67 immunohistochemistry staining, depicting proliferating cells, in MEL270 tumors with or without VS-4718 treatment. E. Tumor volume of OMM1.3 cells *in vivo* with or without VS-4718 treatment, tumor size at the end of the study were measured (mean ± SEM, n=4) (left panel), and hematoxylin and eosin (H&E)- stained sections of representative tumors from each group are shown (right panel). F. Ki67 immunohistochemistry staining of OMM1.3 tumors with or without VS-4718 treatment. G. Representative YAP immunohistochemistry staining of MEL270 tumors with or without VS-4718 treatment. H. Quantification of Fig. 6G, showing fraction of cells with nuclear YAP localization (mean ± SEM, n=3). In all cases ***, $p<0.001$.

KEY RESOURCES TABLE

REAGENT or RESOURCE	SOURCE	IDENTIFIER
Antibodies		
YAP	Cell Signaling Technology, MA	14074
pS127-YAP	Cell Signaling Technology, MA	4911
pS909-LATS1	Cell Signaling Technology, MA	9157
pT1079-LATS1	Cell Signaling Technology, MA	8654
LATS1	Cell Signaling Technology, MA	3477
P-MST1/MST2	Cell Signaling Technology, MA	3681
MST1	Cell Signaling Technology, MA	3682
GAPDH(14C10)	Cell Signaling Technology, MA	2118
α-Tubulin	Cell Signaling Technology, MA	3873
pY	Cell Signaling Technology, MA	9411
HA-tag-HRP	Cell Signaling Technology, MA	2999
HA-tag	Cell Signaling Technology, MA	3724
myc-tag	Cell Signaling Technology, MA	2278
pY397-FAK	Cell Signaling Technology, MA	8556
FAK	Cell Signaling Technology, MA	3285
cleaved PARP	Cell Signaling Technology, MA	9541
p-ERK1/2	Cell Signaling Technology, MA	4370
ERK1/2	Cell Signaling Technology, MA	4696
MOB1	Cell Signaling Technology, MA	13730
pT35-MOB1	Cell Signaling Technology, MA	8699
Gαq(E-17)	Santa Cruz Biotech., CA	sc-393
FAK(C-20)	Santa Cruz Biotech., CA	sc-558
RhoA	Cell Signaling Technology, MA	2117
TRIO(H120)	Santa Cruz Biotech., CA	sc-28564
Rac1	BD Biosciences, CA	610651
pY357-YAP	Abcam, MA	ab62751
LATS2	Bethyl Laboratories, TX	A300–479A
pY26-MOB1A	Signalway Antibody, MA	12878
flag-tag-HRP	Sigma-Aldrich, MO	A8592
Ki67	DAKO, CA	M724029–2
Bacterial strains		
DH5alpha Competent E. coli	BioPioneer, CA	GACC-96
Stbl3 Competent E. coli	Thermo Fisher	C737303
siRNAs		
Non-targeting	Dharmacon, CO	D-001810–0X
GNAQ	Sigma-Aldrich, MO	SASI Hs01 00231793

REAGENT or RESOURCE	SOURCE	IDENTIFIER
Antibodies		
PTK2	Thermo Fisher, MA	s11485
AKT1	Thermo Fisher, MA	s659
MGLL	Thermo Fisher, MA	s22380
MTHFD1	Thermo Fisher, MA	s9032
CDK1	Thermo Fisher, MA	s464
SIRT1	Thermo Fisher, MA	s223591
PSMB5	Thermo Fisher, MA	s11354
TRIO	Dharmacon, CO	L-005047–00-0005
RHOA	Dharmacon, CO	L-003860–00-0005
RAC1	Dharmacon, CO	L-003560–00-0005
LATS1	Sigma-Aldrich, MO	Hs01 00046128
LATS2	Sigma-Aldrich, MO	Hs01 00158803
DNAs		
pCMV-myc-MST1	Addgene	8847
pCMV2-FLAG-SAV1	Addgene	18970
pcDNA3-HA-MOB1	Addgene	32835
pcDNA3-HA-Y26F-MOB1	Generated in-lab	NA
pLENTi-HA-MOB1	Generated in-lab	NA
pLENTi-HA-Y26F-MOB1	Generated in-lab	NA
pGEX-HA-MOB1	Generated in-lab	NA
pGEX-HA-Y26F-MOB1	Generated in-lab	NA
pLVX-T etOne-FLAG-FAK	Generated in-lab	NA
p2xFLAG-CMV2-LATS1	Addgene	18971
8xGTIIC-luciferase	Addgene	34615
REAGENT		
alamarBlue™ Reagent	Grand Island, NY	DAL1100
FAK Kinase Enzyme System	Promega	V1971
YAP1 (Human) Recombinant Protein	Abnova	H00010413-P01
Glutathione Sepharose 4B	GE Healthcare	17–0756-01
N/C Extraction Reagents	ThermoFisher	78833
Software and Algorithms		
ISLE	Lee et al 2018	https://www.github.com/jooslee/ISLE